J. Fluid Mech. (1985), *vol.* 160, *pp.* 385–419
Printed in Great Britain

On the interaction between fundamental and subharmonic instability waves in a turbulent round jet

By REDA R. MANKBADI

Department of Mechanical and Aerospace Engineering, Rutgers University, New Brunswick, NJ 08903

(Received 30 May 1984 and in revised form 28 December 1984)

The spatial interactions between a fundamental instability wave and its subharmonics in a turbulent round jet are studied for 'natural' or forced exit conditions. Time-averaging and conditional-averaging techniques are used to split each flow component into a mean one, a random turbulence one and several wave-like coherent-structure components at fundamental and subharmonic frequencies. The energy equations for the flow components are derived and integrated across the jet. Shape assumptions regarding the radial distributions of each flow component are used to obtain a set of nonlinear ordinary differential equations representing the energy interactions between the coherent components, while interacting with the mean flow and with the background turbulence. Vortex pairing is viewed here as occurring when the subharmonic absorbs energy from the fundamental and from the mean flow and exceeds the fundamental's level to become the dominant instability component. At the proper initial phase difference between the subharmonic and fundamental only the first subharmonic was found to amplify if the fundamental Strouhal number based on diameter is in the range of 0.6–1.0. For higher Strouhal numbers, several subharmonics can amplify. The pairing location moves closer to the nozzle exit with increasing excitation Strouhal number. The time-averaged coherent Reynolds stresses exhibit regions of sign change, indicating a reversal in the direction of energy transfer between the mean flow and the coherent components.

1. Introduction

The existence of large-scale coherent structures in shear flows has now been confirmed by an overwhelming number of observations. The earlier work of Brown & Roshko (1974), Crow & Champagne (1971), Winant & Browand (1974) and Browand & Weidman (1976) demonstrated that the developing flow in both axisymmetric jets and two-dimensional shear layers is dominated by large-scale coherent structures. These structures develop from the exit boundary layer and merge with their neighbours as the shear layer develops downstream. The importance of the subharmonic in vortex pairing has been indicated by Kelly (1967), Corcos & Sherman (1976) and Riley & Metcalfe (1980), among others. Kibens (1980) excited a circular jet with an azimuthally coherent perturbation at the most-amplified frequency of the shear-layer instability. The perturbation organized the large-scale structures in the shear layer into a sequence of successive vortex-pairing stages at fixed streamwise locations. After each pairing, the peak frequency of the spectrum was found to be halved, indicating the amplification of the subharmonic. Ho & Huang (1982) have also shown that for a mixing layer, pairing of vortices is the product of

the subharmonic instability. The pairing location was found to be at the downstream location where the subharmonic saturates. Hence Ho & Huang viewed the subharmonic as a catalyst for vortex pairing. A study of the interaction between an imposed excitation wave and its subharmonics can thus clarify many important concepts regarding vortex pairing.

By viewing the flow as spatially periodic and evolving in time, direct computations of vortex pairing in mixing layers (e.g. Acton 1976; Patnaik, Sherman & Corcos 1976; Knight 1979; Riley & Metcalfe 1980; Corcos & Lin 1984) obtained encouraging results. Numerical simulations of the coalescence of two vortices showed dependency on the phase difference between the fundamental and its subharmonic. The numerical results can be compared with flow visualizations and seem to yield a realistic modelling of the roll-up of the shear layer and vortex pairing in the two-dimensional case. But, as pointed out by Ho & Huerre (1984), the extraction of detailed information regarding the intrinsic scales of motion is more involved.

Coherent structures in mixing layers can be viewed as a composition of interacting instability waves that propagate and amplify in the downstream direction. Linear-stability analysis has been shown to provide some satisfactory results in the initial roll-up of vortices. Freymuth (1966) and Michalke (1965) have shown that the most-amplified frequency scales with the momentum thickness and the jet exit velocity as in experiment. Crow & Champagne (1971) have also shown that linear-stability theory can predict some of the observed features of the preferred mode of an axisymmetric jet. Crighton & Gaster (1976) took the divergence of the jet into consideration and calculated the preferred mode of the velocity profile two diameters downstream of the nozzle. Kelly's (1967) temporal-instability analysis of a spatially periodic mixing layer indicated that the appearance of a frequency half that of the dominant oscillation is due to a secondary instability associated with the periodicity of the flow. Because of the finite-amplitude growth of the fundamental oscillation, energy is transferred from the fundamental to the subharmonic. As a result, the amplification of the subharmonic can exceed that of the most-unstable disturbances associated with the mean flow. These investigations suggest that vortex pairing can be viewed as the interaction between a fundamental instability wave and its subharmonic. Consequently, pairing is viewed here as occurring when the subharmonic absorbs energy from the fundamental and from the mean flow and amplifies to exceed the level of the fundamental and becomes the dominant instability component.

In the present work the interactions between a fundamental wave-like coherent-structure component and its subharmonics are studied for the case of a low-speed turbulent round jet. The coherent structures are idealized as composed of a finite number of instability waves at discrete frequencies. These frequencies are related to each other through the fundamental–subharmonic frequency relations, i.e. the frequencies considered are given by $f/2^n$, where f is the frequency of a fundamental component and $n = 0, 1, 2, 3, \ldots$. In the real situation other frequency components exist and the vortex-pairing pattern can take on different variations depending on the initial conditions. Also, several vortex rings can coalesce together, depending on the excitation conditions. In addition, the amplified first subharmonic $\frac{1}{2}f$ can interact with the fundamental to form the $\frac{3}{2}f$ component, and several other sum and difference frequency components can be generated. However, the problem is simplified here by considering only the pairing between the fundamental and subharmonic components. This simplification is justified by several experimental observations such as those of Kibens (1980, 1981), Zaman & Hussain (1980), Ho & Huang (1982), Baltas & Morris (1984) and Arbey & Ffowcs-Williams (1984), which show that the forced fundamental

and subharmonic components are the dominant frequency components in the initial region of the jet.

Weakly nonlinear theories may be used to study the interaction between the fundamental and subharmonic. But, as pointed out by Huerre (1980), in using weakly nonlinear spatial theories, it is difficult to relate the small-growth-rate assumption to the analysis of vortex pairing when the underlying medium is slowly diverging. The energy-conservation equations, coupled with radial shape assumptions, are used here to derive a set of nonlinear ordinary differential equations describing the energy exchanges between the different flow components. Because of the shape assumptions involved and the finite number of coherent components considered, the energy-integral technique is only approximate. However, it allows study of the strongly nonlinear interactions, whereas weakly nonlinear theories are necessarily restricted to small amplitudes.

2. Formulations

2.1. *Governing equations*

Each flow quantity $g(\boldsymbol{x}, t)$ is split into a mean-flow quantity $\bar{g}(\boldsymbol{x})$, a random fine-grained turbulence $g'(\boldsymbol{x}, t)$ and a set of wave-like coherent-structure components $\tilde{g}(\boldsymbol{x}, t)$. The coherent-structure components are assumed to consist of a single fundamental component, of frequency f, and a series of subharmonic components $\tilde{g}_{f_n}$ of frequencies f_n. The nth subharmonic frequency f_n is related to the fundamental frequency f through the relation $f_n = f/(2)^n$. Thus, following Reynolds & Hussain (1972) and Stuart (1965), each flow quantity can be written in the form:

$$g(\boldsymbol{x}, t) = \bar{g}(\boldsymbol{x}) + g'(\boldsymbol{x}, t) + \tilde{g}_f(\boldsymbol{x}, t) + \sum_{n=1}^{m} \tilde{g}_{f_n}(\boldsymbol{x}, t),$$

where m is the number of subharmonics considered. The conditional average, which is here the phase average with respect to a given frequency, and the usual time average are used to separate the flow into its components. The time average of a random quantity is zero. Each coherent component is assumed to be periodic in time, i.e. $\sim \exp(2\pi i f_n t)$. Therefore the time average of the full quantity produces the mean component, while phase-averaging produces the coherent component plus the mean component. The conditional average with repect to a given frequency will be denoted by $\langle\ \rangle$ and the time-average by $\bar{(\ )}$.

The continuity and Navier–Stokes equations are written in cylindrical coordinates for the full velocity components for imcompressible flows. Time-averaging the full continuity equation produces the mean-flow continuity equation. Successive phase-averaging of the full continuity equation with respect to each frequency produces the continuity equation for each coherent component. The background fine-grained turbulence continuity equation is obtained by subtracting the mean-flow continuity equation and the coherent-structures continuity equations from the full one. The momentum equations are similarly obtained. The process of using phase-averaging to separate the governing equations has been discussed in detail by Hussain & Reynolds (1970), Kendall (1970) and Mankbadi & Liu (1981). The kinetic-energy equation for each flow component is obtained by multiplying the full momentum equations by the corresponding velocity components and time-averaging.

The resulting kinetic-energy equations are simplified by applying the boundary-layer-type approximations (Hinze 1975) to the mean quantities. These approximations

imply that the radial mean-flow velocity V is considered small with respect to the longitudinal one U. The longitudinal gradient of mean quantities is negligible with respect to the corresponding radial gradient. The axisymmetry of the mean flow gives $W = \partial(\bar{})/\partial\phi = 0$. However, no such approximations can be stated regarding the fluctuating quantities prior to averaging. Viscous dissipations of the mean flow and coherent structures are neglected with respect to that of the random turbulence. Triple correlations of random turbulence quantities are neglected, but triple correlations of coherent-structure quantities are kept. After simplification, the energy equations are integrated across the jet, and the diffusion terms vanish. After some manipulations utilizing the continuity equations, the energy equations for the mean flow, coherent-structure components and random turbulence reduce to

mean flow

$$\frac{1}{2}\frac{\mathrm{d}}{\mathrm{d}x}\int_0^\infty U^3 r\,\mathrm{d}r = -\int_0^\infty -\overline{\tilde{u}_f\tilde{v}_f}\frac{\partial U}{\partial r}\,r\,\mathrm{d}r - \sum_{n=1}^{m}\int_0^\infty -\overline{\tilde{u}_{\mathrm{s},n}\tilde{v}_{\mathrm{s},n}}\frac{\partial U}{\partial r}\,r\,\mathrm{d}r - \int_0^\infty -\overline{u'v'}\frac{\partial U}{\partial r}\,r\,\mathrm{d}r, \quad (1a)$$

fundamental

$$\frac{\mathrm{d}}{\mathrm{d}x}\int_0^\infty U\bar{Q}_f r\,\mathrm{d}r = \int_0^\infty -\overline{\tilde{u}_f\tilde{v}_f}\frac{\partial U}{\partial r}\,r\,\mathrm{d}r - \int_0^\infty \bar{\phi}_f r\,\mathrm{d}r - \int_0^\infty \overline{\langle -\tilde{u}_j\tilde{u}_j\rangle_{\mathrm{s},1}\frac{\partial\tilde{u}_{i,f}}{\partial x_j}}\,r\,\mathrm{d}r, \quad (1b)$$

first subharmonic

$$\frac{\mathrm{d}}{\mathrm{d}x}\int_0^\infty U\bar{Q}_{\mathrm{s},1} r\,\mathrm{d}r = \int_0^\infty -\overline{\tilde{u}_{\mathrm{s},1}\tilde{v}_{\mathrm{s},1}}\frac{\partial U}{\partial r}\,r\,\mathrm{d}r - \int_0^\infty \bar{\phi}_{\mathrm{s},1} r\,\mathrm{d}r + \int_0^\infty \overline{\langle -\tilde{u}_i\tilde{u}_j\rangle_{\mathrm{s},1}\frac{\partial\tilde{u}_{i,f}}{\partial x_j}}\,r\,\mathrm{d}r - \int_0^\infty \overline{\langle -\tilde{u}_i\tilde{u}_j\rangle_{\mathrm{s},2}\frac{\partial\tilde{u}_{i,\mathrm{s},1}}{\partial x_j}}\,r\,\mathrm{d}r, \quad (1c)$$

nth subharmonic

$$\frac{\mathrm{d}}{\mathrm{d}x}\int_0^\infty U\bar{Q}_{\mathrm{s},n} r\,\mathrm{d}r = \int_0^\infty -\overline{\tilde{u}_{\mathrm{s},n}\tilde{v}_{\mathrm{s},n}}\frac{\partial U}{\partial r}\,r\,\mathrm{d}r - \int_0^\infty \bar{\phi}_{\mathrm{s},n} r\,\mathrm{d}r + \int_0^\infty \overline{\langle -\tilde{u}_i\tilde{u}_j\rangle_{\mathrm{s},n}\frac{\partial\tilde{u}_{i,\mathrm{s},n-1}}{\partial x_j}}\,r\,\mathrm{d}r - \int_0^\infty \overline{\langle\tilde{u}_i\tilde{u}_j\rangle_{\mathrm{s},n+1}\frac{\partial\tilde{u}_{i,\mathrm{s},n}}{\partial x_j}}\,r\,\mathrm{d}r \quad (n = 2,\ldots,m), \quad (1d)$$

background turbulence

$$\frac{\mathrm{d}}{\mathrm{d}x}\int_0^\infty U\bar{q}r\,\mathrm{d}r = \int_0^\infty -\overline{u'v'}\frac{\partial U}{\partial r}\,r\,\mathrm{d}r + \sum_{n=1}^{m}\int_0^\infty \bar{\phi}_{\mathrm{s},n} r\,\mathrm{d}r + \int_0^\infty \bar{\phi}_f r\,\mathrm{d}r - \int_0^\infty \bar{\epsilon} r\,\mathrm{d}r.$$

$x_i = (x, r, \phi)$ are the coordinates in the axial, radial and azimuthal directions respectively, and $u_i = (u, v, w) = (u_1, u_2, u_3)$ are the corresponding velocity components. U, $\tilde{u}_f$, $\tilde{u}_{\mathrm{s}}$ and u' are the velocities of the mean flow, the coherent fundamental and subharmonic components, and the background turbulence respectively. $\partial/\partial x_j$ is defined as

$$\frac{\partial}{\partial x_j} = \left(\frac{\partial}{\partial x}, \frac{\partial}{\partial r}, \frac{1}{r}\frac{\partial}{\partial\phi}\right).$$

All physical parameters are rendered dimensionless in the following manner. Velocities are normalized by the jet exit velocity U_e, lengths are normalized by the nozzle radius R, and the pressure is normalized by ρU_e^2, where ρ is the fluid mean density. Mean-flow quantities are denoted by capital letters, coherent components by a tilde ($\tilde{}$) and the random turbulence by a prime ($'$). Q and q are respectively the coherent-structure and random-turbulence kinetic energies, defined as

$$Q = \tfrac{1}{2}(\tilde{u}^2+\tilde{v}^2+\tilde{w}^2), \quad q = \tfrac{1}{2}(u'^2+v'^2+w'^2);$$

and ϵ is the viscous dissipation of the random fine-grained turbulence. ϕ_f or $\phi_{s,n}$ are the coherent-structure–random-turbulence interactions, defined as:

$$\phi_f = -\tilde{r}_{ij,f}\tilde{e}_{ij,f}, \quad \tilde{r}_{ij,f} = \langle u_i' u_j' \rangle - \overline{u_i' u_j'},$$

where $\tilde{r}_{ij,f}$ is the wave-induced stress tensor of the coherent component of frequency f, $\tilde{e}_{ij,f}$ is the corresponding strain tensor of the coherent component of frequency f; $\phi_{s,n}$ is similarly defined. Terms in (1) that consist of coherent stresses $\langle -\tilde{u}_i \tilde{u}_j \rangle_{s,n}$ multiplied by coherent strains $\partial \tilde{u}_{i,s,n-1}/\partial x_j$ represent the wave–wave interaction between the f_n and the f_{n-1} components. In obtaining such terms, one should note that, because of the assumed periodicity, the time average of triple correlations of coherent components of frequencies f_k, f_l and f_p is zero unless $f_k \pm f_l = \pm f_p$. Thus for the frequencies considered here ($f_n = f/(2)^n$) the time average of the direct interactions between the f_n component and the other frequency components is zero except for its interactions with f_{n+1} and f_{n-1}.

2.2. *Shape assumptions*

The above system of equations represents the energy interactions between the flow components. To obtain the development of each flow component along the jet several closure assumptions must be made regarding the 'radial shape' distribution of the mean flow, the random turbulence and the coherent structures. These assumptions coupled with (1) provide the fundamental basis for determining the amplitude equations for the nonlinear interactions among the different scales of motion. The mean flow is characterized here by its momentum thickness $\theta(x)$. The coherent-structure components and the random-turbulence component are characterized by their respective energy content across a slice of the jet. The shape assumptions used here follow Mankbadi & Liu (1981, 1984), but are extended to account for the presence of several interacting coherent components. The mean-flow shape is the two-stage hyperbolic-tangent profile proposed by Michalke (1971), which describes the adjustment from a top-hat profile at the nozzle exit to a fully developed jet profile downstream:

$$\frac{U}{U_c} = \left\{ \begin{array}{ll} 1 & (1 \leqslant r < 1-\frac{1}{2}\delta), \\ \frac{1}{2}\left(1+\tanh\dfrac{1-r}{2\theta}\right) & (1-\frac{1}{2}\delta < r) \end{array} \right\} \quad \left(\frac{\theta}{R} < 0.08\right), \tag{2}$$

$$\frac{U}{U_c} = \frac{1}{2}\left(1+\tanh\frac{r^{-1}-r}{4\theta}\right) \qquad \left(\frac{\theta}{R} \geqslant 0.08\right).$$

Moore (1977) has shown that this profile models the circular jet flow in the potential-core region quite well, and it has been used by Crighton & Gaster (1976), Morris (1976) and Plaschko (1979). U_c is the mean velocity at the centreline, δ is the shear-layer thickness and θ is the boundary-layer momentum thickness. The mean

flow is defined here as the time average of the full flow velocity. Thus it is the average over many finite-amplitude vortex structures, and therefore the mean flow is dependent on both the coherent structure and the random turbulence. This dependency is accounted for here through the dependency of the mean flow on the momentum thickness. The momentum thickness is in turn to be determined through the nonlinear interactions between the different flow components, thus coupling the mean flow to the development of both the coherent and turbulent components.

Guided by several experimental observations (e.g. Bradshaw, Ferris & Johnson 1964; Ko & Davies 1971; Davies, Fisher & Barrett 1963), the background random turbulence is modelled as

$$\overline{u_i' u_j'} = a_{ij} E(x) G(\theta) \exp(-\eta^2), \quad \epsilon = a_2 q^3/\delta, \tag{3}$$

where $\eta^2 = (r-1)^2/\theta C_1$; a_{ij} and C_1 are constants given by $a_{11} = 1.0$, $a_{22} = a_{33} = 0.5$, $a_{13} = 0.33$, $a_{13} = a_{23} = 0$, $C_1 = 20$ and $a_2 = 1.5$. $G(\theta)$ is a normalization function such that $E(x)$ is the random-turbulence energy across the jet. The experimental data are used to provide only the radial *shape* of the turbulent Reynolds stresses and their ratios to each other. Both the 'shape' and the ratio are considered to be insensitive to the presence of coherent components in the measured data. The magnitude and the actual local distribution of the turbulent Reynolds stresses, as well as the viscous dissipation $\bar{\epsilon}$, are determined through $E(x)$ and $\theta(x)$, which are both obtained from the nonlinear analysis, thus coupling $\overline{u_i' u_j'}$ and $\bar{\epsilon}$ to the mean flow and to the coherent-structure components.

Shape assumptions for the coherent structure follow Stuart (1958, 1960), Ko, Kubota & Lees (1970) and Liu (1971, 1974) in the form

$$\begin{bmatrix} \tilde{u}_i \\ \tilde{p} \\ \tilde{r}_{ij} \end{bmatrix}_f = A(x) \begin{bmatrix} \hat{u}_i(\theta, r, \omega) \\ \hat{p}(\theta, r, \omega) \\ E(x)\,\hat{r}_{ij}(\theta, r, \omega) \end{bmatrix}_f \exp\left(\mathrm{i} \int_0^x \alpha_{\mathrm{r},f}(\xi)\,\mathrm{d}\xi - \mathrm{i}\omega t + \mathrm{i}\beta_0 \right) + \text{c.c.} \tag{4a}$$

for the fundamental, and

$$\begin{bmatrix} \tilde{u}_i \\ \tilde{p} \\ \tilde{r}_{ij} \end{bmatrix}_{\mathrm{s},n} = B_n(x) \begin{bmatrix} \hat{u}_i(\theta, r, \omega_n) \\ \hat{p}(\theta, r, \omega_n) \\ E(x)\,\hat{r}_{ij}(\theta, r, \omega_n) \end{bmatrix}_{\mathrm{s},n} \exp\left(\mathrm{i} \int_0^x \alpha_{\mathrm{r},n}(\xi)\,\mathrm{d}\xi - \mathrm{i}\omega_n t \right) + \text{c.c.} \tag{4b}$$

for the subharmonic, where c.c. denotes the complex conjugate, α_{r} is the real part of the complex wavenumber α corresponding to the frequency $\omega = 2\pi f$, where f is the fundamental frequency (in Hz), and $\omega_n = \omega/(2)^n$ is the nth subharmonic frequency. The radial shape functions denoted by $\hat{}$ are given by the inviscid linear locally parallel stability theory, and their implicit dependence upon x results from the dependence of the local linear stability theory upon the momentum thickness $\theta(x)$. $A(x)$ and $B_n(x)$ are the fundamental and subharmonic complex amplitudes, to be determined from the nonlinear interaction problem. To a first approximation, $A(x)$ and $B_n(x)$ are taken proportional to

$$\exp\left(-\int_0^x \alpha_i(\xi)\,\mathrm{d}\xi \right)$$

as in the linear theory. β_0 is a prescribed initial phase difference between the fundamental and its subharmonic component. β_0 is introduced here since the work of Patnaik *et al.* (1976), Riley & Metcalfe (1980) and Zhang, Ho & Monkewitz (1984)

showed that the interaction between the fundamental and subharmonic instabilities is dependent on the initial phase difference. In general, β_0 is the initial phase difference between the nth and the $(n-1)$th subharmonic, and can be varied depending on Strouhal number or the order of the subharmonic. A dynamic equation for the wave-induced stresses $\tilde{r}_{ij}$ is obtained as in Mankbadi & Liu (1981) by considering the dynamic equation for $u_i' u_j'$ and subtracting the time-averaged one from the phase-averaged one. The resulting equations for $\tilde{r}_{ij}$ are linearized, producing a set of six simultaneous linear equations to determine the radial distribution of $\hat{r}_{ij}$ across the jet. $\hat{u}_i$ are obtained from the local linear-stability theory and serve as advection velocities in the $\hat{r}_{ij}$ equations. The distribution of energy transfer between the coherent structure and the random turbulence across the jet is then obtained from

$$\tilde{r}_{ij}\,\tilde{e}_{ij} = |A(x)|^2 E(x)\,\hat{r}_{ij}\,\hat{e}_{ij}$$

for each coherent-structure frequency component.

The assumption of using the linear locally parallel stability theory to provide the eigenfunctions as the radial shapes of the coherent components arises from the linearized momentum equation of each coherent component. When this equation is decoupled from the wave-induced stresses it reduces to the linear instability equation. Some arguments and comparisons with observations have been presented in Mankbadi & Liu (1981) for the case of the development of a single coherent component. The validity of this assumption has also been addressed in greater depth by Strange & Crighton (1983). Based on comparisons with measurements, they concluded that, although the amplification rates of the coherent components are not well predicted by the linear theory, the transversal distribution of the coherent quantities is well predicted by the linear theory. The same conclusion has also been reached by Zhang *et al.* (1984) for a mixing layer forced by fundamental and subharmonics. In addition, the eigenfunctions calculated here compared well to the measured velocities and pressure of coherent components obtained by Favre-Marinet & Binder (1979), Ahuja, Lepicovsky & Burrin (1982) and Strange & Crighton (1983).

Because of the non-parallel-flow effects which Crighton & Gaster (1976) and Plaschko (1979), among others, have shown to be significant, the eigenfunctions vary considerably along the jet. To account for this variation, the linear-stability equations are solved at each axial location to provide the local eigenfunctions along the jet corresponding to a given frequency. The solution of the linear-stability problem follows Michalke's (1971) method for the amplified solution. Beyond the neutral point the damped solution is obtained by taking the problem to the complex-r plane and following a rectangular contour of integration as in Morris (1976). The eigenfunctions $\hat{u}_i$ and $\hat{p}$ are normalized in such a manner that $|A(x)|^2$ and $|B_n|^2$ become the kinetic energies for the fundamental and subharmonic components respectively. The nonlinear interactions between the several flow components thus control the levels of the coherent structures and the random turbulence through $|A|^2$, $|B|^2$ and E, and control the radial shape distributions of all flow components through θ.

2.3. *The nonlinear interaction*

Upon substituting the shape assumptions discussed in §2.2 into the energy equations (1), the following set of ordinary differential equations for θ, $|A|^2$, $|B_n|^2$ and E is obtained:

mean flow

$$\frac{1}{2}\frac{\mathrm{d}I_1(\theta)}{\mathrm{d}\theta}\frac{\mathrm{d}\theta}{\mathrm{d}x} = -I'_{\mathrm{Rs}}(\theta)E - \tilde{I}_{\mathrm{Rs}}(\theta, St)|A|^2 - \sum_{n-1}^{m} \tilde{I}_{\mathrm{Rs}}(\theta, S_n)|B_n|^2, \qquad (5a)$$

fundamental

$$[I_2(\theta, St)\,|A|^2] = \tilde{I}_{\mathrm{Rs}}(\theta, St)\,|A|^2 - I_{\mathrm{wt}}(\theta, St)\,|A|^2 E - I_{\mathrm{ww}}(\theta, St, S_1)\,|A|\,|B_1|^2, \quad (5b)$$

first subharmonic

$$\frac{\mathrm{d}}{\mathrm{d}x}[I_2(\theta, S_1)\,|B_1|^2] = \tilde{I}_{\mathrm{Rs}}(\theta, S_1)\,|B_1|^2 - I_{\mathrm{wt}}(\theta, S_1)\,|B_1|^2 E + I_{\mathrm{ww}}(\theta, St, S_1)\,|A|\,|B_1|^2 - I_{\mathrm{ww}}(\theta, S_1, S_2)\,|B_1|\,|B_2|^2, \quad (5c)$$

nth subharmonic

$$\frac{\mathrm{d}}{\mathrm{d}x}[I_2(\theta, S_n)\,|B_n|^2] = \tilde{I}_{\mathrm{Rs}}(\theta, S_n)\,|B_n|^2 - I_{\mathrm{wt}}(\theta, S_n)\,|B_n|^2 E + I_{\mathrm{ww}}(\theta, S_{n-1}, S_n)\,|B_{n-1}|\,|B_n|^2 - I_{\mathrm{ww}}(\theta, S_n, S_{n+1})\,|B_n|\,|B_{n+1}|^2 \quad (n = 2, 3, \ldots, m), \quad (5d)$$

random turbulence

$$\frac{\mathrm{d}}{\mathrm{d}x}[I_3(\theta)\,E] = I'_{\mathrm{Rs}}(\theta)\,E + I_{\mathrm{wt}}(\theta, St)\,|A|^2 E + \sum_{n=1}^{m} I_{\mathrm{wt}}(\theta, S_n)\,|B_n|^2 E - I_\epsilon(\theta)\,E^{\frac{3}{2}}, \quad (5e)$$

where $St = fd/U_{\mathrm{e}}$ is the fundamental Strouhal number. f is the frequency, d is the nozzle-exit diameter, U_{e} is the exit velocity. The nth subharmonic Strouhal number S_n is defined as $S_n = St/(2)^n$. The initial conditions for (5) are $\theta(0) = \theta_0$, $|A(0)|^2 = |A|_0^2$, $|B_n(0)|^2 = |B_n|_0^2$, and $E(0) = E_0$.

Because of the shape assumptions discussed in §2.2, integrals involving only the mean-flow velocity profile and mean fine-grained turbulence stresses are functions of the local momentum thickness alone, while integrals involving the large-scale structure depend not only on θ but also on St and the order of the subharmonic. The integrals I_1, I_2, I_3, I'_{Rs}, I_{wt} and I_ϵ are the same as in Mankbadi & Liu (1981) for the development of a single monochromatic coherent component. The mean-flow energy-advection integral is defined as

$$I_1(\theta) = \int_0^h U^3 r\,\mathrm{d}r,$$

where h is the outer edge of the shear layer. Note that (5a) is actually an equation for $\mathrm{d}\theta/\mathrm{d}x$ with $\mathrm{d}I_1(\theta)/\mathrm{d}\theta < 0$. The large-scale-structure energy-advection integral is

$$I_2(\theta, St) = \int_0^h U(|\hat{u}|^2 + |\hat{v}|^2)\,r\,\mathrm{d}r$$

and the fine-grained-turbulence energy-advection integral is

$$I_3(\theta) = G(\theta) \int_0^h U \exp(-\eta^2)\,r\,\mathrm{d}r.$$

The production integrals of the fine-grained turbulence and large-scale structure are respectively

$$I'_{\mathrm{Rs}}(\theta) = (-a_{12})\,G(\theta) \int_0^h \exp(-\eta^2)\,\frac{\partial U}{\partial r}\,r\,\mathrm{d}r,$$

$$\tilde{I}_{\mathrm{Rs}}(\theta, St) = -2 \int_0^h \mathrm{Re}\,(\hat{u}\hat{v}^*)\,\frac{\partial U}{\partial r}\,r\,\mathrm{d}r,$$

where ( )* denotes the complex conjugate of ( ). The large-scale-structure turbulence-energy-exchange integral is

$$I_{\rm wt}(\theta, St) = -2\int_0^h \mathrm{Re}\left\{\hat{r}^*_{xx}(\mathrm{i}\alpha\hat{u}) + \hat{r}^*_{rr}\hat{v}' + \frac{\hat{r}^*_{\phi\phi}\hat{v}}{r} + r^*_{xr}(\mathrm{i}\alpha\hat{v} + \hat{u}')\right\} r\,\mathrm{d}r,$$

where ( )′ denotes differentiation with respect to r. The fine-grained-turbulence dissipation integral is

$$I_\epsilon(\theta) = \frac{a_2}{a_3\theta} G_1^4(\theta)\int_0^h \exp\left(-\tfrac{3}{2}\eta^2\right) r\,\mathrm{d}r.$$

$I_{\rm ww}(\theta, S_{n-1}, S_n)$ represents the interactions between fundamental and subharmonic, or generally between the $(n-1)$th subharmonic and the nth subharmonic, and is defined as

$$\left.\begin{aligned} I_{\rm ww} &= -2\,\mathrm{Re}\left\{\exp\left[\mathrm{i}\beta_0 + \mathrm{i}\int_0^x (\alpha_{r,\,n-1}(\xi) - 2\alpha_{r,\,n}(\xi))\,\mathrm{d}\xi\right] I_{\rm fs}(\theta, S_n, S_{n-1})\right\}, \\ I_{\rm fs} &= \int_0^h \left\{\hat{u}^*_{s,\,n}\hat{u}^*_{s,\,n}\frac{\partial\hat{u}_{s,\,n-1}}{\partial x} + \hat{u}^*_{s,\,n}\hat{v}^*_{s,\,n}\left(\frac{\partial\hat{u}_{s,\,n-1}}{\partial r} + \frac{\partial\hat{v}_{s,\,n-1}}{\partial x}\right) + \hat{v}^*_{s,\,n}\hat{v}^*_{s,\,n}\frac{\partial\hat{v}_{s,\,n-1}}{\partial r}\right\} r\,\mathrm{d}r. \end{aligned}\right\} \quad (6)$$

$i_{\rm ww}$ appears with opposite signs in (5*b*) and (5*c*) or in (5*c*) and (5*d*) and represents the energy cascade between the fundamental and the subsequent subharmonics. The real and imaginary parts of $I_{\rm fs}$ are shown in figure 1. The effective phase difference between the fundamental and subharmonic is thus given by

$$\beta_0 + \int_0^x ([\alpha_{r,\,n-1}(\xi) - 2\alpha_{r,\,n}(\xi)]\,\mathrm{d}\xi,$$

as in (6). This phase difference is calculated here based on the linear locally parallel stability theory, which provides $\alpha_{r,\,n}(\xi)$ and $\alpha_{r,\,n-1}(\xi)$ along the jet for a given frequency. This assumption is supported by Drubka's (1981) measurements of the phase angle of each coherent component along the jet. His measurements indicated that the phase angle varies linearly along the jet. This linear behaviour of the phase angle has also been observed by Laufer & Yen (1983). Hence the phase difference can be given approximately by the linear theory, although the amplitudes of the two waves are given by the nonlinear theory.

In (5*a–e*) the left-hand sides are the energy advections of each flow component by the mean flow. The first term on the right-hand side of (5*a*) appears with an opposite sign to the first term in (5*e*) and is the random-turbulence energy production by the mean flow. $I'_{\rm Rs}(\theta)$ is a positive decreasing function of θ, indicating one direction of energy transfer from the mean flow to the random turbulence. The second and subsequent terms in (5*a*) appear with opposite signs to the first terms in (5*b–d*) and represent the energy transfer from the mean flow to the fundamental and the subharmonics respectively. For the amplified linear-stability solutions $I_{\rm Rs}$ is positive, while for the damped solution $I_{\rm Rs}$ is negative, indicating damping of coherent-structure components by the return of their energies to the mean flow at some downstream stations. With $\mathrm{d}I_1(\theta)/\mathrm{d}\theta < 0$ (5*a*) indicates that the shear layer grows as a result of the productions of the coherent and random components. Equations (5*b–d*) indicate that the coherent-structure component grows by absorbing energy from the mean flow and decays through random-turbulence dissipation. The wave–wave interaction terms in (5*b–d*) can act as production or damping terms, depending on the order of the subharmonic considered and the choice of the initial phase difference β_0. In (5*b*)

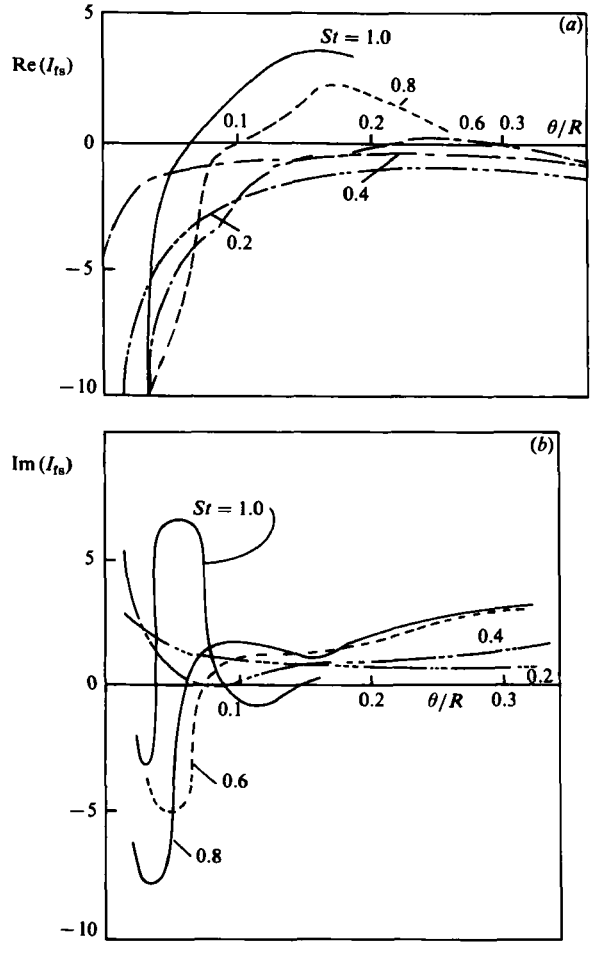

FIGURE 1. Wave–wave interaction integral I_{fs}, for several Strouhal numbers: (*a*) real part; (*b*) imaginary part.

for the fundamental of frequency f the interactions with higher harmonics, i.e. $2f, 4f, \ldots$, are neglected for the sake of simplyifing the problem. For the case of excitation at high Strouhal numbers, the harmonics of the forced component will be in the stable region. Therefore they will be damped and can be neglected. This is not true for low or moderate Strouhal numbers, where the harmonics can amplify and become relevant. However, the observations of Baltas & Morris (1984) and Zaman & Hussain (1980) have indicated that for this low to moderate Strouhal number range the harmonics of the forced component are much smaller than the first subharmonic of the fundamental. Therefore the present analysis is restricted to the interaction of the fundamental with its subharmonic and excludes the interaction with the higher harmonic.

Equation (5*e*) indicates that the random turbulence gains energy from the mean flow and from the coherent-structure components and loses energy through viscous dissipation.

With the shape assumptions discussed in §2.2, the integrals involved in (5) can be calculated for a given Strouhal number as a function of θ. Once the initial conditions

θ_0, $|A|_0^2$, $|B_n|_0^2$ and E_0 are fixed, the development of $\theta(x)$, $|A(x)|^2$, $|B_n(x)|^2$ and $E(x)$ along the jet can be obtained. By taking the initial levels of the fundamental and its subharmonics to be weak enough to match the corresponding levels in the 'natural' unforced jet, one can follow the development of the several flow components along a 'natural' jet. By taking the initial level of the fundamental so as to match the condition of forcing at a single frequency, while keeping the other initial conditions as in the unforced case, one can follow the development of the flow components under forced conditions.

3. The role of Strouhal number on vortex pairing

The solution of the nonlinear interaction problem (5) is subject to the initial conditions of θ_0, E_0, $|A|_0^2$, $|B_n|_0^2$ as well as the Strouhal number, which controls the interaction integrals. θ_0 is determined from the exit velocity profile, which is a function of whether the exit boundary layer is laminar or turbulent. E_0, the initial random-turbulence energy density, can be related to the exit turbulence-velocity components through (3). $|A|_0^2$, the initial energy density of the forced or natural fundamental component of the Strouhal number St, can be related to the corresponding exit velocity through (4a). Similarly, the initial energy density of the subharmonic components $|B_n|_0^2$, $n = 1, 2, \ldots, m$, are related to the corresponding exit velocities through (4b). The experimental observations of Laufer & Zhang (1983), Husain & Hussain (1983), Zaman & Hussain (1980) and Kibens (1980) show the initial momentum thickness to be about (0.002–0.005)d for laminar exit boundary layers and about (0.005–0.007)d for turbulent exit boundary layers. The exit centreline longitudinal random-turbulence velocity component is about 0.1–0.5 % of U_e, and the unexcited coherent-structure exit centreline longitudinal velocity components are about 0.01–0.1 % or U_e. $|A|_0^2$ depends on the excitation level. From such data one can determine θ_0, E_0, $|A|_0^2$ and $|B_n|_0^2$. In order to examine the role of Strouhal number on vortex pairing, (5) is solved under excitation conditions at several Strouhal numbers that raises the initial level of the corresponding $|A|_0^2$, while keeping the other initial conditions as in the unexcited case. For a given set of initial conditions and Strouhal number, (6) shows that the fundamental–subharmonic interaction integral is also a function of the initial phase difference β_0 between the fundamental and its first subharmonic or that between the nth and the $(n-1)$th subharmonics. The development of the fundamental and its subharmonics will consequently be dependent on the choice of these parameters, as the observation of Zhang *et al.* (1984) for a mixing layer has indicated. The natural uncontrolled initial subharmonic components can exist with any phase differences with respect to the fundamental. The forced fundamental will act as an amplifier to its first subharmonic, and the degree of amplification will depend on β_0, as will be discussed in §5. Since vortex pairing is viewed here as the amplification of the subharmonic β_0 will be taken as the value that produces maximum subharmonic amplification at a given excitation Strouhal number. For all of the Strouhal-number range considered $\beta_0 \approx 0$ was found to produce maximum initial subharmonic amplification very close to the jet exit, as in the two-dimensional case. However, the optimum β_0 for the maximum subharmonic's peak energy downstream was found to vary from $\frac{3}{2}\pi$ at low Strouhal numbers to $\beta_0 = 0$ at high Strouhal numbers (§5). Thus, for each Strouhal number considered, β_0 is taken here as the value that produces maximum subharmonic amplification.

The development of the forced fundamental component and its subharmonics are shown in figure 2 (*a–g*) for fundamental Strouhal numbers of 0.2, 0.4, 0.6, 0.8, 1.0,

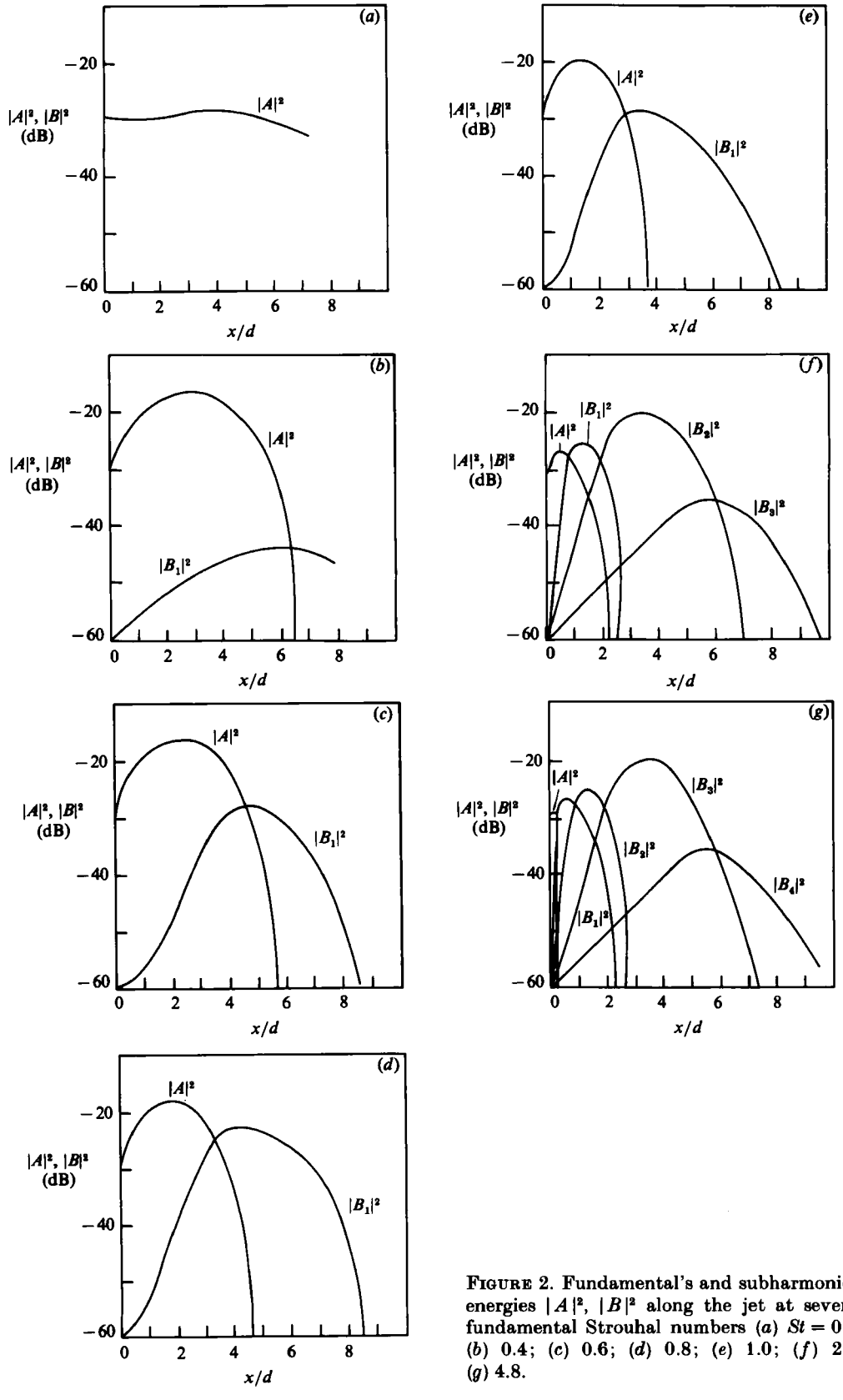

FIGURE 2. Fundamental's and subharmonic's energies $|A|^2$, $|B|^2$ along the jet at several fundamental Strouhal numbers (*a*) $St = 0.2$; (*b*) 0.4; (*c*) 0.6; (*d*) 0.8; (*e*) 1.0; (*f*) 2.4; (*g*) 4.8.

2.4 and 4.8 respectively. The presence of four subharmonics of the fundamental is considered in solving (5). The initial conditions for the solutions of (5) were fixed at $\theta_0 = 0.003d$, $u' = 0.3\,\%\ U_e$ at the exit jet centreline. $|B_n|_0^2$ was fixed at 10^{-6} for all subharmonics, which corresponds to exit velocities of about $0.1\,\%\ U_e$. $|A|_0^2$ was fixed at 10^{-3}, which corresponds to exit velocities of about $0.03U_e$. At $St = 0.2$ figure 2(*a*) shows that the forced fundamental grows at a slow rate, its streamwise lifespan is considerably large, but no subharmonic can be detected. At $St = 0.4$ figure 2(*b*) shows an increase in the growth rate of the forced fundamental, but its streamwise lifespan decreases with increasing Strouhal number. Only the first subharmonic is amplified, with a peak at $x/d \approx 6$, but its energy level is much less than that of the fundamental or the background turbulence. For the Strouhal number range 0.6–1.0 figures 2(*c–e*) shown that the energy level of the first subharmonic is comparable to that of the fundamental, but the energy levels of the second, third and fourth subharmonics are still negligible and are therefore not shown in the figures. As (5*b*) indicates, the fundamental first grows as it absorbs energy from the mean flow, and subsequently decays by giving its energy to the background turbulence and to its first subharmonic. The subharmonic grows by absorbing energy from the fundamental and from the mean flow, and subsequently decays by dissipating its energy to the background turbulence. Figures 2(*c–e*) show that the locations of the fundamental's and subharmonic's peaks move closer to the nozzle exit with increasing excitation Strouhal number. Defining the location of vortex pairing is a subjective problem. Ho & Huang (1982) defined the pairing location being where the subharmonic saturates. Since pairing is viewed here as occurring when the subharmonic's energy exceeds that of the fundamental, the location of pairing can alternatively be defined as where the subharmonic's energy becomes equal to that of the fundamental. Whichever of the two definitions is adopted, one can infer from figure 2 that the location of pairing moves closer to the jet exit with increasing Strouhal number. This is consistent with Ho & Huang's (1982) observations for a plane shear layer.

Excitation at the Strouhal-number range 2.4–4.8 produces several subharmonics, as figures 2(*f, g*) indicate. At $St = 2.4$ figure 2(*f*) indicates that three vortex pairings can be formed, corresponding to the amplification of the first, second and third subharmonics of Strouhal numbers 1.2, 0.6 and 0.3 respectively. The forced fundamental grows by absorbing energy from the mean flow, and subsequently, as it decays, it amplifies its first subharmonic. The first subharmonic grows by absorbing energy from the fundamental and from the mean flow, and subsequently, as it decays, it amplifies the next subharmonic. The next subharmonic behaves similarly. The location of the subharmonic's peak coincides with the location where the fundamental is rapidly decaying. At Strouhal number 4.8 figure 2(*g*) shows similar behaviour, and four vortex pairings can be formed, corresponding to the appearance of the first, second, third and fourth subharmonics of Strouhal numbers 2.4, 1.2, 0.6 and 0.3 respectively. For an exit momentum thickness of $\theta_0 = 0.003d$, the Strouhal numbers based on θ_0, $St_\theta = f\theta_0/U_e$, are 0.0072 and 0.144 for $St = 2.4$ and 4.8 respectively. Therefore the Strouhal-number range of figure 2(*f, g*) is close to the natural shear-layer instability frequency. The calculated amplification of several subharmonics in figure 2(*f, g*) is in qualitative agreement with several observations, including those of Drubka (1981), Laufer & Zhang (1983) and Husain & Hussain (1983). The theory also shows that the location of the subharmonic's peak coincides with the rapid decay of the fundamental, as in Ho & Huang's (1982) observation for a plane shear layer. The calculated streamwise regions for which each frequency is the dominant component are also in qualitative agreement with the corresponding regions of Wlezien & Kibens' (1984) measured passage frequency along the jet after each pairing.

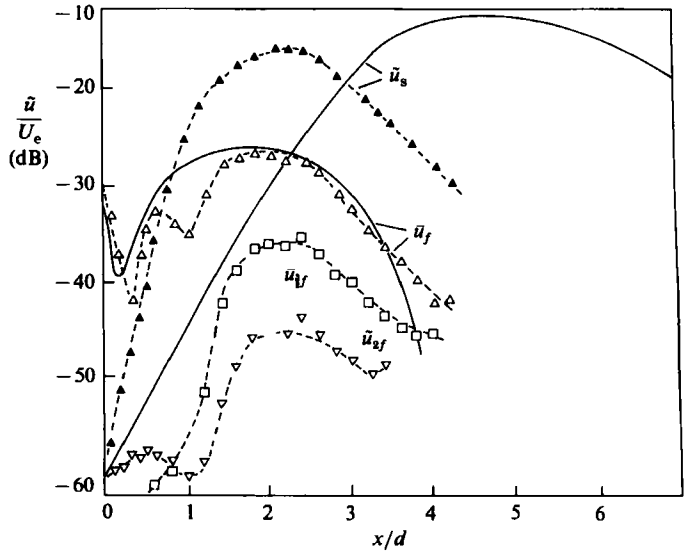

FIGURE 3. Predicted development of the fundamental's and first subharmonic's centreline axial velocity components $\tilde{u}_f$ and $\tilde{u}_s$ respectively at $St = 0.8$, in comparison with Zaman & Hussain's (1980) measurements at $St = 0.85$.

To present quantitative comparisons between theory and observation, (5) is solved for the same initial conditions as in Zaman & Hussain's (1980) experiment. The predicted centreline streamwise evolutions of the fundamental and first subharmonic axial velocity components are shown in figure 3 for $St = 0.8$ in comparison with the observations at $St = 0.85$ for a laminar exit boundary layer. The excitation level is taken as in the observation where the forced centreline axial velocity component at the jet exit is $0.03U_e$, which determines $|A|_0^2$. The observed exit momentum thickness is $\theta_0 = 0.003d$. The measured exit centreline axial velocity components of the background turbulence and the subharmonic coherent structure are 0.3 % U_e and 0.1 % U_e respectively, which determines E_0 and $|B_n|_0^2$. In figure 3 both theory and observations show that the fundamental is the dominant component close to the jet exit, and that it grows to a peak around $x/d = 1.75$, and decays at $x/d \approx 4$. The theory predicts the first subharmonic to amplify to about 17 % of U_e, almost the same level as in the observations. However, while the observations show the subharmonic to peak around $x/d = 2.5$, the predicted peak location is about $x/d = 5$. This can be attributed to the fact that at $x/d = 1$ the observations show the $\frac{3}{2}f$ component to amplify and to reach a non-negligible level at $x/d = 2$. The amplification of this $\frac{3}{2}f$ component is due to a second interaction mechanism in which the f and the $\frac{1}{2}f$ components interact to form the $f+\frac{1}{2}f$ component. This mechanism is not accounted for in the present model. The amplification of the $\frac{3}{2}f$ component results in draining energy from the subharmonic and would cause its earlier saturation, as in the experiment. Comparing the calculated and measured growths of the subharmonic also shows that the calculated growth rate of the subharmonic is less than the observed one. This is attributed to the presence of the shear-layer mode of pairing in the experiment, which is not accounted for here. As will be discussed later, the presence of an initial shear-layer mode can cause further amplification in the subharmonic ($S_1 = 0.4$) of the fundamental forced component of $St = 0.8$.

The predicted growth of the first subharmonic of $S_1 = 0.3$, 0.4 and 0.5 when the

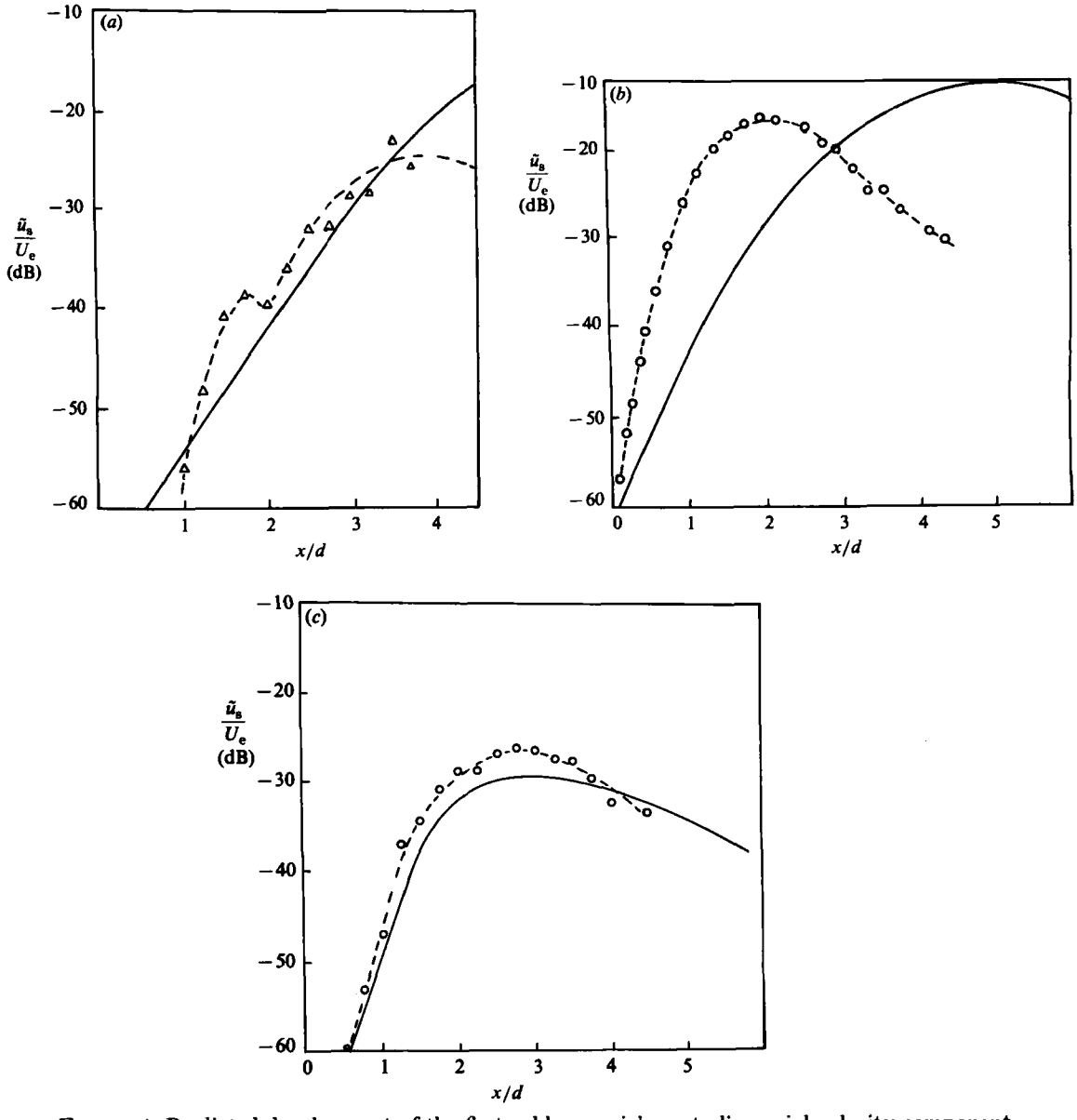

FIGURE 4. Predicted development of the first subharmonic's centreline axial velocity component $\tilde{u}_s$, in comparison with Zaman & Hussain's (1980) data; exit laminar boundary layer, excitation level 3%: (*a*) $St = 0.6$; (*b*) 0.8 (theory), 0.85 (experiment); (*c*) 1.0.

jet is excited at $St = 0.6$, 0.8 and 1.0 respectively is shown in figure 4 in comparison with Zaman & Hussain's (1980) observed first subharmonic when the jet is excited at $St = 0.6$, 0.85 and 1.0. The initial first-subharmonic level is taken so as to match the initial measured level in each case. The other initial conditions are kept as those of figure 3. Figure 4 shows that the theory predicts the same level of the subharmonic's amplification, but the predicted location of the subharmonic peak is farther downstream. In the case of a turbulent exit boundary layer the predicted growth of the first subharmonic is shown in figure 5 in comparison with the corresponding

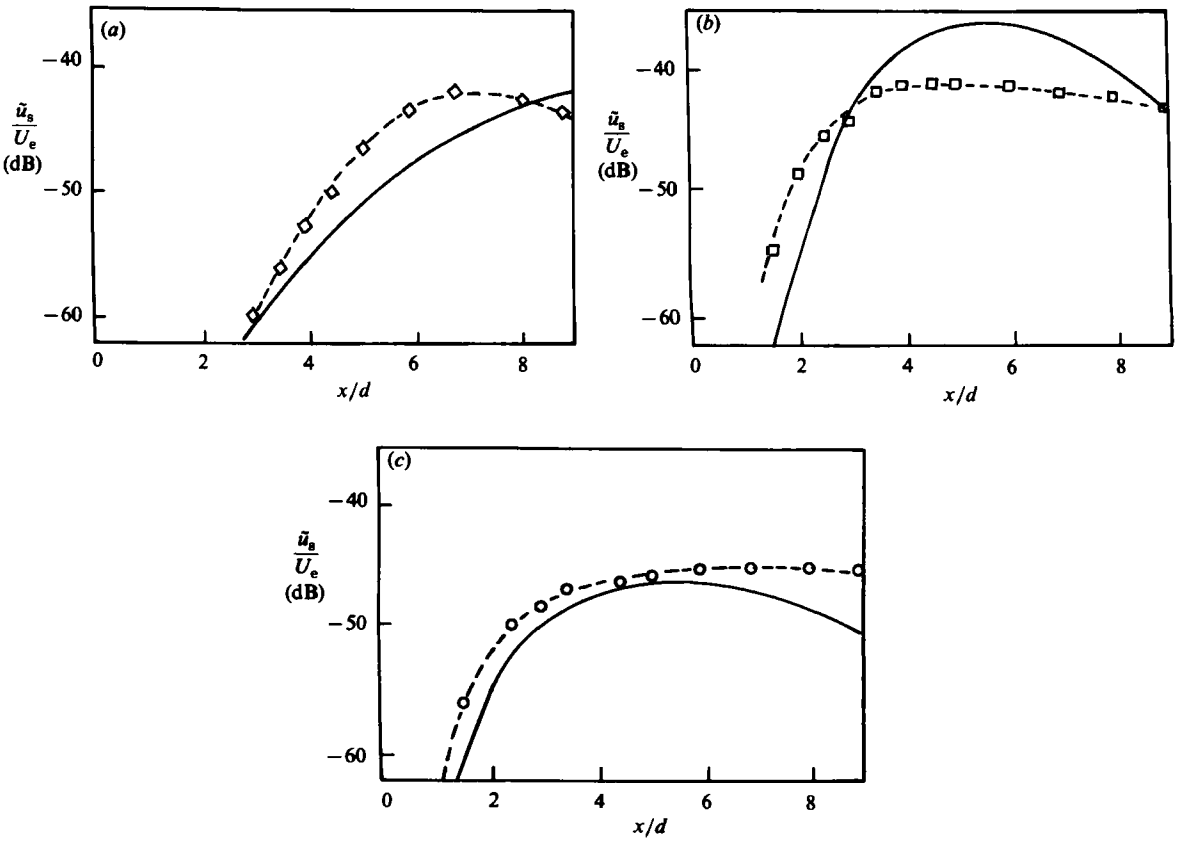

FIGURE 5. Predicted development of the first subharmonic's centreline axial velocity component $\tilde{u}_s$, in comparison with Zaman & Hussain's (1980) data; exit turbulent boundary layer, excitation level 1 %: (*a*) $St = 0.40$ (theory), 0.44 (experiment); (*b*) 0.8 (theory and experiment); (*c*) 1.0 (theory), 1.13 (experiment).

observations of Zaman & Hussain (1980) for several excitation Strouhal numbers. The initial conditions are taken as in the experiment: an excitation level of 1 % U_e, $\theta_0 = 0.0025d$, $u' = 0.3\,\%\ U_e$ and the subharmonic's initial axial velocity component equals $0.01\,\%\ U_e$. Figures 4 and 5 show that the agreement between theory and observations is better in the turbulent exit-boundary-layer case than in the laminar case. This can be explained as follows. In the present formulation the presence of an initial natural shear-layer mode of pairing and its coupling to the low-Strouhal-number components are not considered. As will be discussed in §4, if the jet is excited at a moderate Strouhal number the amplification of the corresponding subharmonic is dependent on its initial level. The presence of an initial natural shear-layer mode of pairing alters the initial level of several subharmonics, including the subharmonic that will interact downstream as the first subharmonic of the moderate-Strouhal-number forced fundamental (see figures 2*f*, *g*). Thus the presence of an initial natural shear-layer mode can thus alter the subharmonic's amplification when the jet is excited at moderate Strouhal numbers. In the laminar exit-boundary-layer case (figure 4) the observations indicate the presence of an initial natural shear-layer mode. Therefore the comparison between theory and observations are less satisfactory. In the turbulent exit-boundary-layer case (figure 5) the observations show that the

initial natural shear-layer mode is removed. Therefore the agreement between theory and observations is more satisfactory in the turbulent exit-boundary-layer case than in the laminar case.

Zaman & Hussain (1980) adopted the view that for a circular jet rolled-up vortex rings undergo pairing under two distinctive conditions of excitation: the 'shear-layer mode', and the 'jet-column mode'. The shear-layer mode is the one similar to that of the plane mixing layer, and is observed for the circular jet when the excitation Strouhal number based on the exit momentum thickness was about 0.012 and the exit boundary layer was laminar. It involves pairing of the near-exit thin vortex rings. Zaman & Hussain defined the jet-column mode as the one involving pairing of the thick vortex rings further downstream. It is observed for both laminar and turbulent exit boundary layers when the excitation Strouhal number based on diameter is about 0.85. They concluded that the jet-column mode of pairing can form independently of the shear-layer mode, or as a result from evolution of the shear-layer mode, or when the jet is excited directly in the jet-column mode. The predicted growth of the first subharmonic at the excitation-Strouhal-number range $St = 0.6$–1.0, shown in figures 2 (*c–e*), without accounting for the presence of an initial shear-layer mode is in agreement with Zaman & Hussain's conclusion that the jet-column mode can occur independently of the shear-layer mode. On the other hand, figure 2 shows that the calculated development of the fundamental and its subharmonics indicates that there is a continuum of response behaviour as the excitation Strouhal number is increased. The particularly pronounced amplification of the first subharmonic when the jet is excited at fundamental Strouhal number $St = 0.8$ is due to the fact that the subharmonic's amplification is due to both the mean-flow instability mechanism and the fundamental–subharmonic interaction mechanism. It is known that the most-preferred frequency associated with the mean-flow profile of a circular jet is of Strouhal number about 0.4 (see e.g. Gutmark & Ho 1983). When the jet is excited at a fundamental Strouhal number of 0.8 the corresponding first subharmonic has a Strouhal number of 0.4, which is the 'preferred' Strouhal number of the jet. Therefore its amplification is particularly pronounced. Since pairing is viewed here as the subharmonic amplification, the particularly pronounced amplification of the subharmonic at the jet-column mode can thus be attributed to the instability of the mean-flow profile in addition to its interaction with the forced fundamental.

4. The effect of excitation level

In §3 the nonlinear interaction between the fundamental and subharmonic was found to result in amplifying the subharmonic. Altering the development of the fundamental through excitation can thus result in altering the interaction process. The effect of the forcing level on the development of the fundamental and subharmonic is examined here by varying the initial level of $|A|^2$, while keeping the other initial conditions of (5) fixed at $\theta_0 = 0.003d$, $u' = 0.3\,\%$ and $|B|_0^2 = 10^{-6}$. At $St = 0.8$ the growth of the forced fundamental and its first subharmonic is shown in figure 6 for several excitation levels. Figure 6(*a*) shows that the peak of the fundamental increases nonlinearly with the excitation level, but its growth rate is reduced. The fundamental is saturated at $|A|_0^2 = 0.01$, corresponding to an exit forced velocity of about $10\,\%\ U_e$. The peak of the fundamental moves closer to the nozzle exit and its streamwise lifespan is reduced as the excitation level increases. Since the initial level of the subharmonic is fixed at $|B|_0^2 = 10^{-6}$ for all the excitation levels considered, the change in the growth rate of the subharmonic (shown in figure 6*b*) is mainly due to

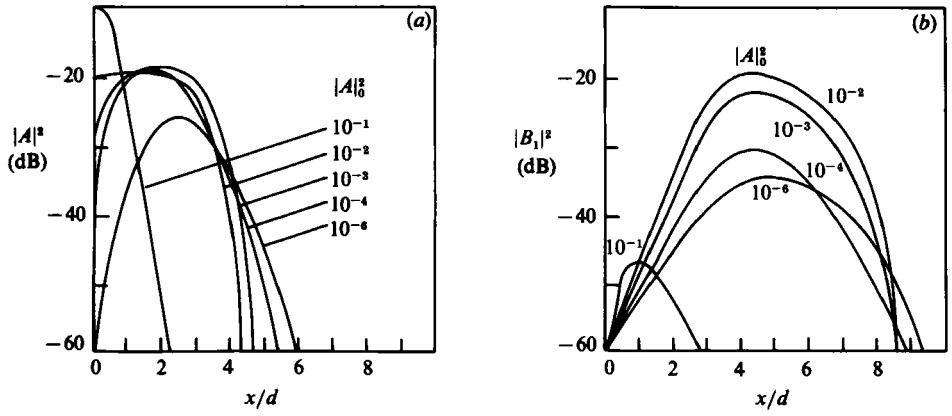

FIGURE 6. Effect of excitation level $|A|_0^2$ on the development of the fundamental and subharmonic at $St = 0.8$ and $|B_n|_0^2 = 10^{-6}$: (*a*) fundamental's energy $|A|^2$; (*b*) first subharmonic's energy $|B_1|^2$.

the change in the fundamental's level. For low level of excitation at $|A|_0^2 = 10^{-6}$ the subharmonic's growth is dominated by its interaction with the mean flow, and is thus mainly due to the mean-flow instability mechanism. As the excitation level increases, energy is pumped from the fundamental to the subharmonic, through the $|A|\,|B|^2 I_{ww}$ term. This increases the subharmonic's initial growth rate. The subharmonic peak moves closer to the nozzle exit with increasing excitation level, as observed by Laufer & Yen (1983). As $|A|_0^2$ increases to 0.01, the subharmonic peak level also increases. But for $|A|_0^2 = 0.1$, although the initial growth rate of the subharmonic is increased, its peak is considerably reduced. This is a result of the excessive drain of the mean-flow energy by the fundamental, and hence less energy is available for the subharmonic. Thus there is an optimum excitation level that will produce maximum subharmonic amplification, which is consistent with Monkewitz's (1982) conclusion for a two-dimensional shear layer.

Figure 6 (*b*) also clarifies the mechanism of the subharmonic's growth resulting from the fundamental versus the one resulting from the mean-flow instability. By taking the case of $|A|_0^2 = 10^{-6}$ so as to correspond to negligible fundamental–subharmonic interactions, figure 6 (*b*) shows that the subharmonic peak corresponds to about $\tilde{u} = 1.8\%\ U_e$, while for strong fundamental–subharmonic interactions, as in $|A|_0^2 = 0.01$, the subharmonic peak increases considerably to about $\tilde{u} = 10\%\ U_e$. This indicates the strong subharmonic amplification mechanism resulting from the finite-amplitude growth of the fundamental. Figures 6 (*a*, *b*) also show that the peaks of the fundamental and subharmonic move closer to the jet exit with increasing excitation level, as in Laufer & Yen's (1983) observation. Recalling that pairing is viewed here as the subharmonic's amplification, one can conclude from figure 6 that the location of pairing also moves closer to the jet exit with increasing excitation level. Figure 6 also shows that weak vortex pairing can occur at the nominally unexcited conditions of $|A|_0^2 = 10^{-6}$ and that the vortex pairing is more pronounced with increasing excitation level. This is in qualitative agreement with Acton's (1980) results. Acton modelled the large eddies in an axisymmetric jet using an inviscid discrete-vortex model. For $St = 0.5$ her results showed that as the forcing level was increased the large-eddy formation was very regular and there was an immediate big-eddy structure at the forcing wavelength. Figure 6 also shows that for excessive forcing levels as $|A|_0^2 = 0.1$ (corresponding to a forcing frequency of about 30% U_e) the vortex pairing can be suppressed as in Reynolds & Bouchard's (1981) experiment.

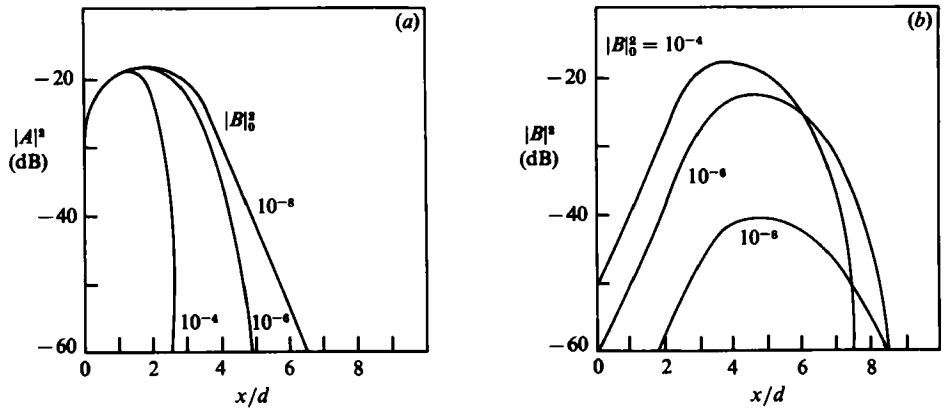

FIGURE 7. Effect of initial level of the subharmonic $|B_n|_0^2$ on the development of the fundamental and subharmonic at $St = 0.8$ and $|A|_0^2 = 10^{-3}$: (*a*) fundamental's energy $|A|^2$; (*b*) first subharmonic's energy $|B_1|^2$.

To examine the role of the nonlinear fundamental–subharmonic interactions on the fundamental, the development of the fundamental and subharmonic is shown in figure 7 for several initial levels of the first subharmonic while keeping the initial level of the fundamental fixed at $|A|_0^2 = 10^{-3}$. The excitation Strouhal number is 0.8, $\theta_0 = 0.003d$ and $u' = 0.3\%\ U_e$ at $x/d = 0$. The subharmonic's initial level was varied from a negligible level of $|B|_0^2 = 10^{-8}$ to a moderate level of $|B|_0^2 = 10^{-4}$. Figure 7 shows that the initial growth of the fundamental is independent of the subharmonic, but its decay rate increases rapidly with increasing level of the subharmonic. The fundamental–subharmonic interaction is thus significant to the fundamental only in its decay stage. Equation 5(*b*) shows that the role of the fundamental–subharmonic interaction on the development of the fundamental is important only when $|B|^2/|A|$ is roughly of order one, and this is true only at later downstream stages where $|B|^2$ is large enough. Figure 7 also shows that the peaks of the fundamental and subharmonic move closer to the jet exit with increasing initial level of the subharmonic. Hence the location of pairing moves closer to the nozzle exit with increasing initial level of the subharmonic. Thus the location and the strength of the vortex pairing are also dependent on the initial level of the subharmonic. In an experimental facility this initial level of the subharmonic is dependent on the background disturbances. These disturbances change the initial subharmonic's level and its subsequent pairing with the fundamental, and can thus explain the observed irregularity or jitter in vortex pairing.

Another means of isolating the fundamental–subharmonic interaction mechanism from the mean-flow instability mechanism is to artificially decouple the growth of the fundamental from that of the subharmonic. This can be done by setting the fundamental–subharmonic interaction integral I_{ww} to zero in (5). Thus the fundamental and subharmonics interact simultaneously with the mean flow and the background turbulence, but not directly with each other. The simultaneous presence of the fundamental and subharmonic still indirectly affects the growth of each of them through their individual interactions with the mean flow and with the background turbulence. Thus a decoupled case corresponds to the simultaneous presence of the coherent components under artificially non-pairing conditions. The growths of the fundamental and subharmonic in the pairing and non-pairing cases are shown in figure 8 for $St = 0.8$ and initial conditions of $|A|_0^2 = 0.001$, $|B|_0^2 = 10^{-6}$, $\theta_0 = 0.003d$ and $u' = 0.003U_e$. The figure clearly indicates that the fundamental–subharmonic

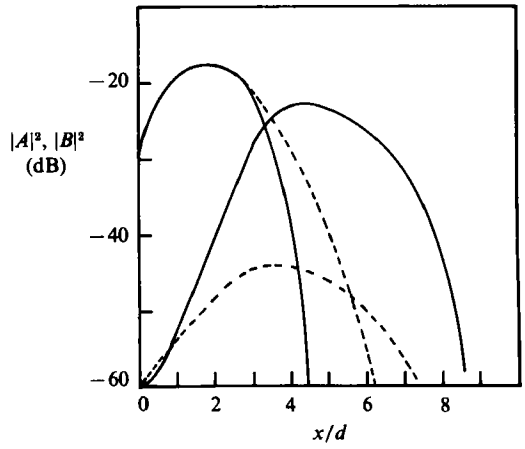

FIGURE 8. Effect of the fundamental–subharmonic interaction on the development of the fundamental and subharmonic at $St = 0.8$, $|A|_0^2 = 10^{-3}$, $|B_n|_0^2 = 10^{-6}$: ——, fundamental–subharmonic interaction included; – – – –, decoupled.

interaction mechanism results in acceleration of the decay of the fundamental and in enhancement of the amplification of the subharmonic. The peak energy of the subharmonic, with the fundamental–subharmonic interaction taken into account, is about two orders of magnitude greater than its peak due to the mean-flow instability mechanism alone. The figure also shows that the fundamental–subharmonic interaction mechanism is much more pronounced for the subharmonic than for the fundamental. This can be explained through (5), which shows that the relative significance of the fundamental–subharmonic interaction term is proportional to $|B|^2/|A|$ for the fundamental and to $|A|$ for the subharmonic. Since $|B|$ is initially much smaller than $|A|$, the effect of the fundamental–subharmonic interaction is less pronounced for the fundamental than for the subharmonic.

The effect of forcing level at a high Strouhal number of $St = 4.8$, corresponding to $St_\theta = 0.0144$, is shown in figure 9. The initial conditions are $\theta_0 = 0.003$, $u' = 0.003U_e$, $|B_n|^2 = 10^{-6}$ and the forcing level is varied from $|A|_0^2 = 10^{-6}$ to $|A|_0^2 = 10^{-3}$. For all forcing levels considered, the figure shows the amplification of four subharmonics. This can be interpreted as the formation of four vortex pairings. The figure shows that the growth rate of the fundamental decreases with increasing excitation level. The fundamental saturates as the excitation level increases to $|A|_0^2 = 10^{-3}$. This is in accordance with Laufer & Zhang's (1983) experiment, in which a jet is forced close to the natural instability frequency at low forcing level. They found that the peak of the fundamental remains relatively constant with increasing the excitation level. The figure also shows that, as the excitation level increases, the location of the fundamental's peak moves closer to the jet exit, which is consistent with Freymuth's (1966) and Laufer & Yen's (1983) measurements. Figure 9 also shows that the levels of the subharmonic slightly increase with increasing initial level of the fundamental. The peaks of the subharmonics and hence the location of pairing, move closer to the jet exit. For $St = 2.0$ Acton's (1980) results showed that with increasing the forcing level there is a much stronger response, and the large eddy disappeared within one diameter. Figure 9 also shows that the energy cascades from the fundamental to the subsequent harmonics. This effect is more pronounced at the first subharmonic, and diminishes at the higher-order subharmonics. As the initial energy level of the fundamental increases from 10^{-6} to 10^{-3}, the peak energy of the first subharmonic

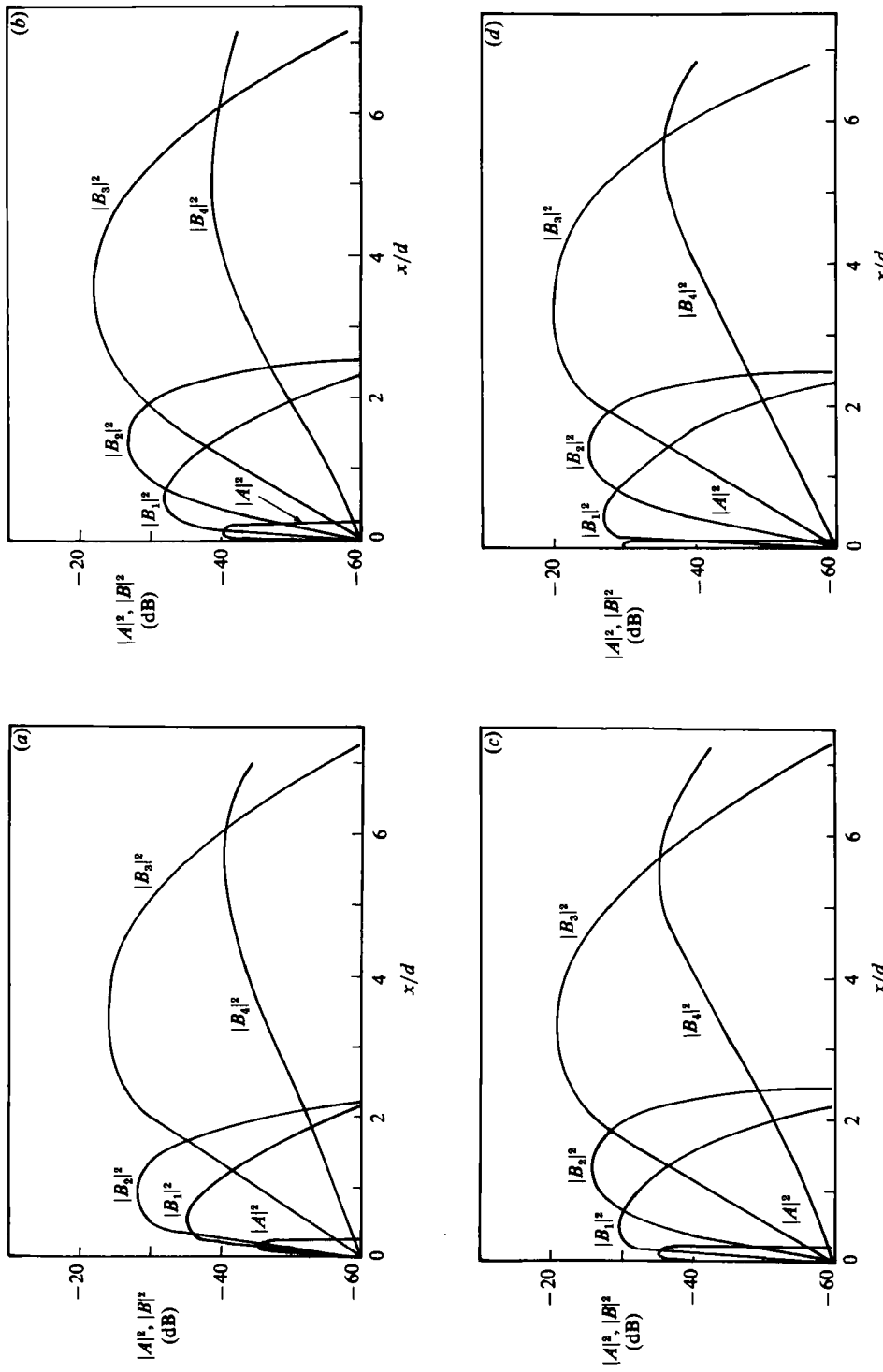

FIGURE 9. Effect of excitation level on the development of the fundamental and subharmonic coherent components in the shear-layer mode; $St = 4.8$ ($St_\theta = 0.0144$), $|B_n|_0^2 = 10^{-6}$: (*a*) $|A|_0^2 = 10^{-6}$; (*b*) 10^{-6}; (*c*) 10^{-4}; (*d*) 10^{-3}.

increases by a factor of six, while the peak energy of the fourth subharmonic increases by only a factor of three.

Figure 9 also explains the link between the 'shear-layer mode' and the 'jet-column mode' of pairing. In figure 7 the vortex pairing at $St = 0.8$, typical of the jet-column mode, was found to be dependent on the initial level of its first subharmonic, which has a Strouhal number of 0.4. Considering the shear-layer mode at $St = 4.8$ (figure 9) the fourth subharmonic ($S_4 = 0.3$) can be taken as representative of the first subharmonic of the jet-column mode at Strouhal number 0.4. Figure 9 shows that the level of this subharmonic S_4 slightly increases in the initial region of the jet as a result of excitation at the shear-layer mode. If the initial level of the subharmonic is increased, its subsequent downstream pairing with the fundamental in the jet-column mode will also be enhanced. Thus, although the jet-column mode is not necessarily a consequence of the shear-layer mode, the two modes are inextricably coupled.

5. The effect of the initial phase difference between fundamental and subharmonic

Equation (5) shows that the nonlinear interaction between fundamental and subharmonic is governed by I_{ww}, defined in (6), which can be written as

$$I_{ww} = 2\,|I_{fs}|\cos(\gamma+\beta), \tag{7}$$

where $|I_{fs}|$ and γ are respectively the magnitude and phase of I_{fs}, and I_{fs} is equal to I_{ww} at $\beta = 0$, where β is defined by (6) as

$$\beta = \beta_0 + \int_0^x [\alpha_{r,\,n-1}(\xi) - 2\alpha_{r,\,n}(\xi)]\,d\xi.$$

The real and imaginary parts of I_{fs} were shown in figure 1. The effective wave–wave interaction term is thus a combination of both the real and imaginary parts of I_{fs}, depending on β. For $\beta = 0$ and π, only the real part of I_{fs} contributes to I_{ww} and the sign of I_{ww} reverses when β changes from 0 to π. Similarly, for $\beta = \frac{1}{2}\pi$ and $\frac{3}{2}\pi$, only the imaginary part of I_{fs} contributes to the wave–wave interaction process, with the sign reversing between $\beta = \frac{1}{2}\pi$ and $\frac{3}{2}\pi$. Since β is dependent on β_0, and noting that in (6) the wavenumber $\alpha_{r,\,n}$ is about half $\alpha_{r,\,n-1}$, the choice of β_0 considerably influences the development of the coherent components. In §§3 and 4, β_0 was chosen as the value that produces maximum subharmonic amplification. To study the effect of β_0 on the interaction process, the developments of the first subharmonic and the fundamental axial velocity components, at several values of β_0, are shown in figures 10 and 11 for $St = 0.8$ and 2.4 respectively. The initial conditions for the solution of the nonlinear equations (5) in figures 10 and 11 are taken as $\theta_0 = 0.003d$, $u' = 0.3\,\%\ U_e$, $\tilde{u}_f = 3\,\%\ U_e$ and $\tilde{u}_s = 0.1\,\%\ U_e$. In order to isolate the phase effect, only the first subharmonic of the fundamental is considered in the calculations of figures 10 and 11. The development of each component in the decoupled case where the fundamental–subharmonic interaction is neglected is also shown as dotted lines in the figures. Both figures 10(*a*) and 11(*a*) indicate that the initial growth of the fundamental and its peak are independent of β_0. During the decay stage of the fundamental, figures 10(*a*) and 11(*a*) show that β_0 has a pronounced effect on accelerating the decay of the fundamental. This damping effect is proportional to the subharmonic's amplification shown in figures 10(*b*) and 11(*b*), and is due to the extraction of the fundamental's energy for the growth of the subharmonic.

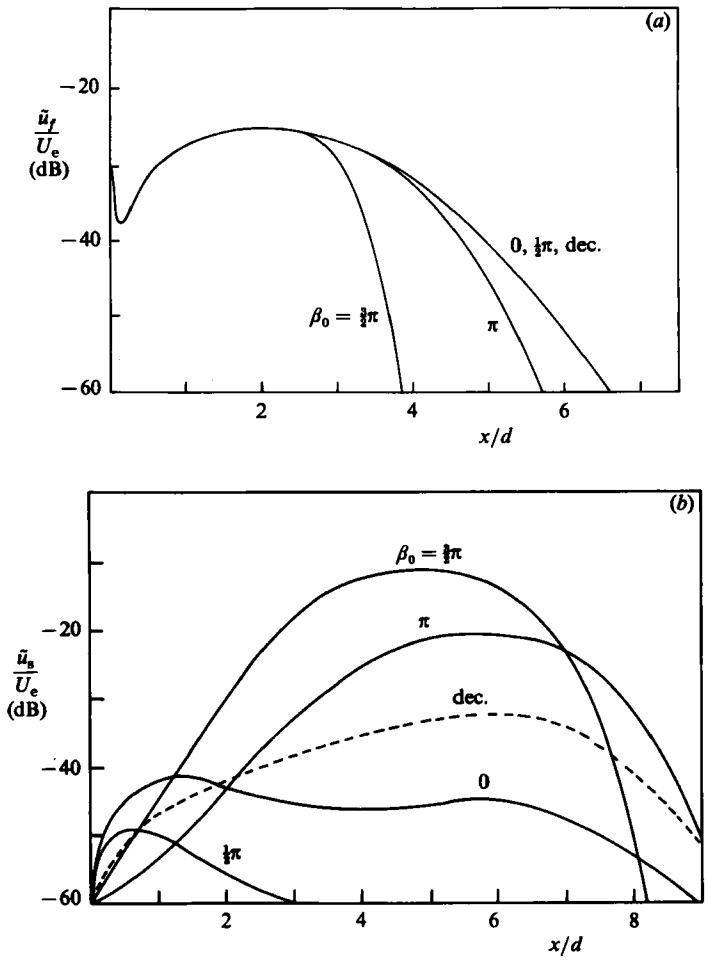

FIGURE 10. Effect of the initial phase difference β_0 on the growth of the fundamental and subharmonic at $St = 0.8$, $\tilde{u}_f = 3\%\ U_e$ at $x = 0$: (*a*) fundamental's centreline axial velocity component; (*b*) first subharmonic centreline axial velocity component.

Both figures 10(*b*) and 11(*b*) show that the phase difference β_0 has a pronounced effect on the growth of the subharmonic. Close to the nozzle exit, at either $St = 0.8$ or 2.4, the subharmonic's initial growth rate is enhanced if β_0 is close to π, i.e. out of phase. The subsequent downstream effect of β_0 on the development of the subharmonic at $St = 0.8$ is different from that at $St = 2.4$. For $St = 2.4$ the streamwise lifespan of the subharmonic is short. Thus an initially higher amplification rate results in subsequently higher peak, and for high Strouhal numbers the subharmonic peak is maximum, as is the initial growth rate, when $\beta_0 = 0$. For moderate Strouhal numbers as in $St = 0.8$, the subharmonic's streamwise lifespan is much longer. As a result of the initially higher growth rate the subharmonic ($S_1 = 0.4$) at $\beta_0 = 0$ reaches its peak sooner and drains more energy from the mean flow. Consequently, less mean-flow energy is available for its subsequent downstream growth along the jet. Thus, though the initial growth rate of the subharmonic is maximum when the two waves are in phase, the subsequent subharmonic peak is maximum when $\beta_0 = \frac{3}{2}\pi$ for $St = 0.8$.

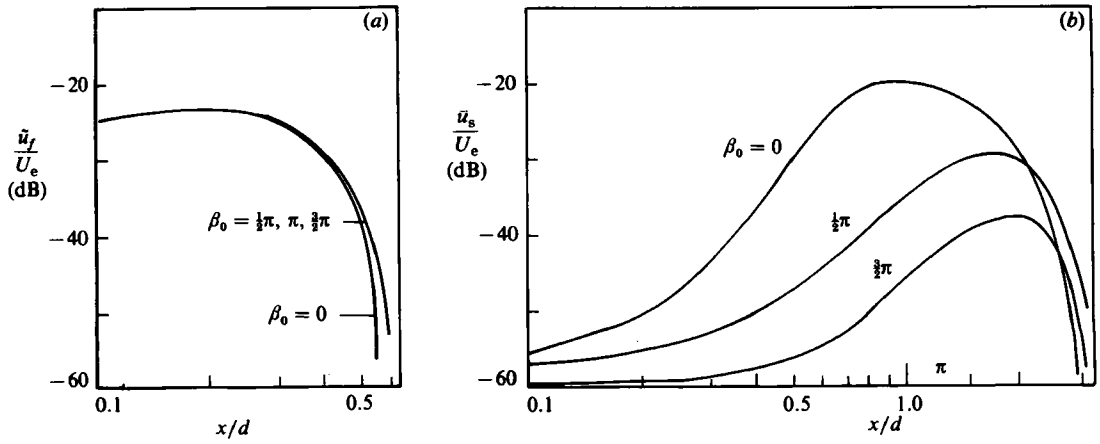

FIGURE 11. Effect of the initial phase difference β_0 on the growth of the fundamental and subharmonic at $St = 2.4$, $\tilde{u}_f = 3\,\%\ U_e$ at $x = 0$.

The initial region of a round jet close to the nozzle exit is similar to a two-dimensional shear layer. Therefore some of the features obtained in figures 10 and 11 can be qualitatively compared with those of the two-dimensional shear layer. Zhang *et al.* (1984) forced a mixing layer at both the fundamental and subharmonic frequencies. The amplification rates of the fundamental were found to be weakly dependent on β_0 as obtained here in figures 10(*a*) and 11(*a*). The measured subharmonic's growth rates were found to decrease by as much as 30 % when β_0 was varied between 0 and π, as the present theory has shown in figure 11(*b*). The effect of the phase difference on the growth of the subharmonic can also be seen in the numerical results of Patnaik Sherman & Corcos (1976), Riley & Metcalfe (1980) and Corcos & Lin (1984) for the case of a stratified mixing layer. Their results showed the pairing or the shedding interaction to be dependent on the phase difference.

With the role of the initial phase difference on the growth of the subharmonic now established, one can conclude that the jet instability acts as an amplifier not only with respect to selective frequencies, but also with respect to selective phase differences between fundamental and subharmonic. In natural uncontrolled conditions, several subharmonic components at a given frequency can exist with several random phase differences with respect to the fundamental. The mean flow acts as a first amplifier that will amplify or suppress the subharmonic, depending on its frequency. The fundamental instability wave associated with the mean-flow profile then acts as a second amplifier that will amplify or reduce the subharmonic, depending on its arbitrary initial phase difference with respect to the fundamental. For a given frequency the most-amplified subharmonic is thus the one with the proper phase difference. This can be the cause of the observed jitter in the location or strength of pairing. If the uncontrolled subharmonic component at the nozzle exit is at the proper phase difference, it will produce a strong pairing at some downstream location. But, if the phase difference is not the optimum one, the strength of pairing will be reduced and its location will be altered.

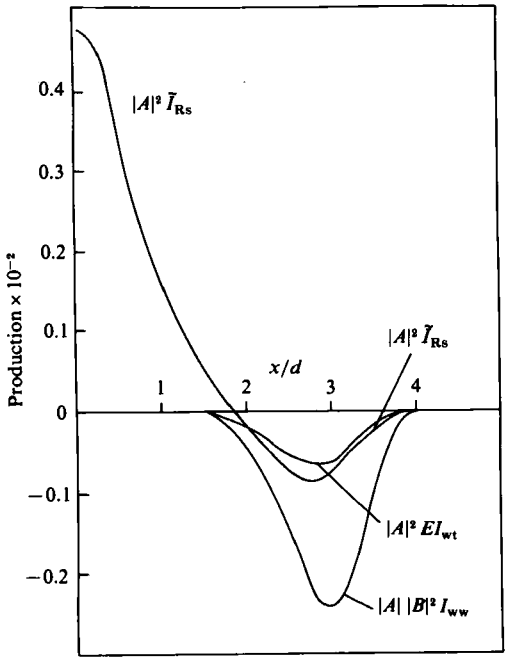

FIGURE 12. Energy-exchange terms of the fundamental at $St = 0.8$ and excitation level $\tilde{u}_f = 3\,\%\ U_e$.

6. The energy-transfer mechanism for vortex pairing

In order to understand the pairing process, the energy transfer responsible for the development of the fundamental and its subharmonic is examined here for $St = 0.8$ and 4.8. The energy exchanges at $St = 0.8$ are presented in figures 12 and 13 for excitation conditions $\tilde{u}_f = 3\,\%\ U_e$, $u' = 0.3\,\%\ U_e$, $\tilde{u}_s = 0.1\,\%\ U_e$ and $\theta_0 = 0.003d$.

Figure 12 shows the production of the fundamental component by the mean flow $|A|^2 \tilde{I}_{Rs}$, the turbulence damping $|A|^2 EI_{wt}$ and the energy drained from the fundamental to the subharmonic $|A|\,|B_1|^2 I_{ww}$. In the initial region of the jet the production of the fundamental by the mean flow is the dominant term, and therefore the fundamental grows. But for $x > 1.5d$ three mechanisms contribute to the decay of the fundamental.

(i) *Turbulence damping* ($|A|^2 EI_{wt}$), where the random turbulence intensity has now increased enough to play an important role in the decay of the fundamental. For a mixing layer between two streams, Browand & Latigo (1979) observed that when the initial boundary layer was turbulent, the shear layer's growth rate was found to be initially less than when the initial boundary layer was laminar. They interpreted this reduction in the growth rate as a result of the coherent structure damping through the introduced turbulence, which is in accordance with the present turbulence damping mechanism.

(ii) *The fundamental–subharmonic interaction mechanism* ($|A|\,|B_1|^2 I_{ww}$), through which the subharmonic grows by absorbing energy from the fundamental.

(iii) *The production of the fundamental by the mean flow*, which becomes negative at some downstream stations, indicating energy transfer from the coherent component back to the mean flow. The linear-stability theory predicts a damped solution for this

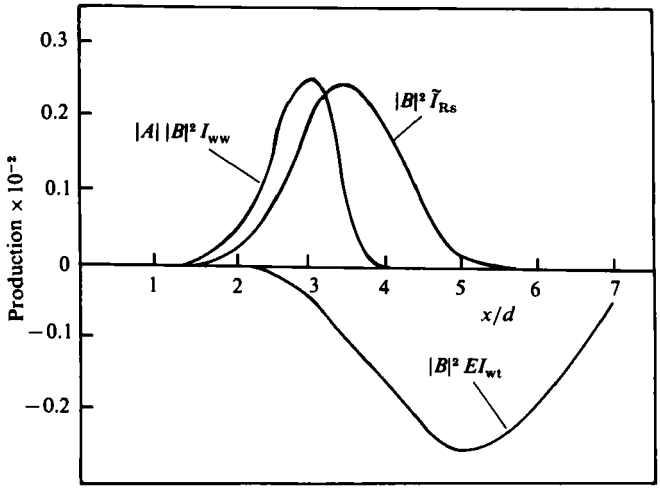

FIGURE 13. Energy-exchange terms of the first subharmonic at $St = 0.8$ and excitation level $\tilde{u}_f = 3\%\ U_e$.

Strouhal number at large values of θ. In the present analysis the sign of the production of coherent structure is determined by

$$\tilde{I}_{Rs} = \int_0^h -\overline{\hat{u}\hat{v}}\frac{\partial U}{\partial r}\, r\, dr.$$

$\tilde{I}_{Rs}$ is calculated here based on the linear-stability solution, and therefore is negative when the linear solution is damped, which is physically consistent. Since the mean shear $\partial U/\partial r$ does not change sign along the jet, negative production is here a result of negative coherent stresses. Browand (1980) was the first to comment on the significance of these negative Reynolds stresses and their relation to the pairing process. These negative Reynolds stresses have also been observed by Oster & Wygnanski (1982) for the two-dimensional shear layer and by Zaman & Hussain (1980) for the round jet. For a two-dimensional shear layer, Browand & Ho (1983) interpret the negative Reynolds stress as a result of the tilt of the vorticity distribution. If the tilt is upstream on the low-speed side, the resulting momentum flux is away from the mixing layer. Consequently the turbulence energy is decreased. For the unexcited shear layer the tilt is usually downstream on the low-speed side, and therefore negative Reynolds stress is unlikely to be produced. If the shear layer is forced the vortex structure is controlled, and the tilt can result in negative Reynolds stresses.

The energy-exchange terms for the subharmonic are shown in figure 13 with the same ordinate scale as that for the fundamental in figure 12. The figure shows that the subharmonic energy terms are initially negligible with respect to those of the fundamental for $x/d < 1.5$. Therefore these terms have little effect on the initial growth of the fundamental. However, for $x/d > 1.5$ the figure shows that the subharmonic's energy interactions are of the same order as that of the fundamental. For $x/d > 1.5$ the production of the subharmonic by the fundamental is of the same order as that of the subharmonic's production by the mean flow. Thus, the fundamental amplifies the subharmonic in two ways: first it absorbs energy from the mean flow in the initial region of the jet, and subsequently, as it decays, it pumps this energy to the subharmonic through $|B_1|^2 |A| I_{ww}$. Secondly, the enhancement

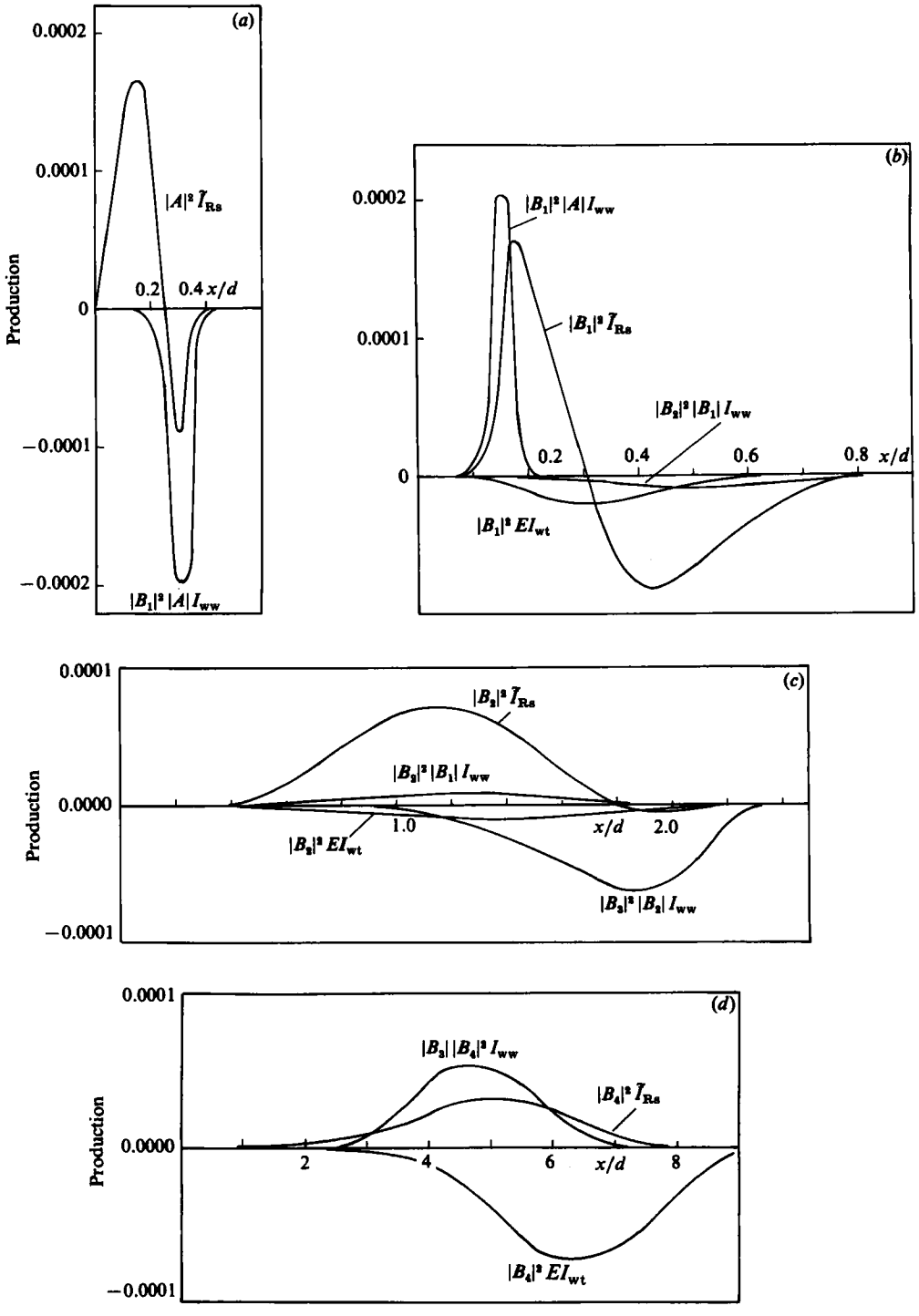

FIGURE 14. Energy exchange terms of the fundamental and subharmonics at $St = 2.4$ and excitation level $\tilde{u}_f = 3\,\%\ U_e$: (*a*) fundamental; (*b*) first subharmonic; (*c*) second subharmonic; (*d*) fourth subharmonic.

of the subharmonic's level through the fundamental–subharmonic interaction acts as a catalyst for enhancing the direct production of the subharmonic by the mean flow ($|B|^2 \tilde{I}_{Rs}$). The two mechanisms combined result in considerable amplification of the subharmonic. The subharmonic subsequently decays basically through the turbulence-damping mechanism.

At $St = 4.8$ the energy-exchange terms are shown in figure 14 for the fundamental and its subharmonics. The initial conditions are $\theta_0 = 0.003d$, $u' = 0.3\,\%\ U_e$ and the initial longitudinal velocities of the subharmonics are $0.1\,\%\ U_e$. The initial longitudinal velocity of the fundamental is $1\,\%\ U_e$. Figure 14 (*a*) shows that the fundamental grows as a result of its production by the mean flow and decays as a result of generating its first subharmonic and as a result of its mean-flow production being negative. The effect of random turbulence on damping the fundamental is negligible with respect to the two former damping mechanisms. The first subharmonic initially grows as a result of the energy gained from the mean flow and from the fundamental, as figure 14 (*b*) indicates. The first subharmonic subsequently decays through the three damping mechanisms: mean-flow negative production, generating the subsequent subharmonic, and damping through the random turbulence. The subsequent subharmonics grow through the same mechanisms as figures 14 (*c*, *d*) indicate. However, while the 'negative production' is a significant damping mechanism for the fundamental and first subharmonic, the turbulence damping becomes the dominant mechanism for the decay of the higher subharmonic, as in the fourth subharmonic shown in figure 14 (*d*).

7. The effect of the fundamental–subharmonic interactions on the random turbulence

In the present model the coherent components control the development of the random turbulence in two ways. First, they absorb energy from the mean flow and pump it to the random turbulence through the coherent-structure–random-turbulence interaction terms. Secondly, by altering the growth rate of the mean flow, the energy available to the random turbulence through direct mean-flow production $I'_{Rs} E$ is also altered. The first mechanism always tends to enhance the random turbulence. In the second mechanism $I'_{Rs}(\theta)$ is a decreasing function of θ, thus the higher spreading rate produced by the coherent structure decreases $I'_{Rs}(\theta)$, which represents the potential for the turbulence production by the mean flow. But the actual production EI'_{Rs} is a function of E, and therefore depends on the initial conditions of E_0, $|A|_0^2$, $|B|_0^2$, θ_0 and the Strouhal number. Thus, in principle, the second mechanism can have either an amplification or suppression effect on the random turbulence. The fundamental–subharmonic interaction is a third indirect mechanism which controls the development of the random turbulence through altering the above two mechanisms. Controlling vortex pairing through excitation can thus lead to either an amplification or suppression of the random turbulence.

For the unexcited case the initial level of coherent structure is weak, and the random-turbulence production is mainly due to the mean flow. Figure 15 shows the predicted distribution of the centreline axial random-turbulence root-mean-square value of u' in comparison with the measurement of Drubka (1981) and Husain & Hussain (1980). The initial conditions for the solution of (5) are taken from the corresponding experiment in each case. The two figures show good agreement between theory and experiment for the initial region of the jet. However, farther downstream for $x/d > 7$, the present theory tends to underestimate the turbulence

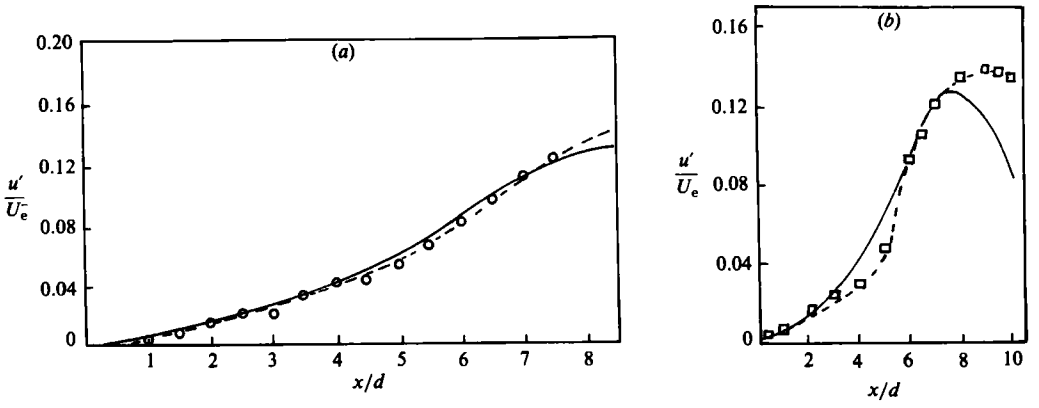

FIGURE 15. Calculated random turbulence centreline axial velocity component in comparison with experimental data: (*a*) comparison with Drubka's (1980) data; (*b*) comparison with Husain & Hussain's (1980) data.

intensity, which can be attributed to two factors. First, the present turbulence model relies on a radial shape distribution for the turbulent Reynolds stresses, with a peak at $r = \frac{1}{2}d$. This is true in the initial region of the jet. but farther downstream this peak is observed to move toward the centreline. Thus the present turbulence model may not be reliable farther downstream in the fully developed region. Secondly, the phase-averaged experimental results of Drubka (1981) and Husain & Hussain (1980) were not high-pass filtered to eliminate the low-frequency components. Their random components resulting from phase averaging may contain low-frequency variability, which is not included in the calculated random components.

7.1. *Turbulence enhancement due to excitation*

The observations of Crow & Champagne (1971), Chan (1974), Moore (1977), Zaman & Hussain (1980) and Kibens (1980) showed that excitation at moderate Strouhal numbers produces amplification of the fluctuating components. In order to examine the role of excitation on enhancing the random turbulence, the centreline development of the axial random turbulence velocity component is shown in figure 16 for the unforced case, and for 3 % forcing at $St = 0.8$. Note that only the random component of the fluctuating axial velocity is shown in the figure. The total fluctuating component, which is usually the one measured in experiment, consists of the random turbulence as well as the fundamental and subharmonic coherent components,

$$(\overline{u_t'^2})^{\frac{1}{2}} = (\overline{u'^2} + \overline{\tilde{u}_f^2} + \overline{\tilde{u}_s^2})^{\frac{1}{2}},$$

which is greater than u' alone. Figure 16 shows that the excitation enhances the jet turbulence in accordance with the above observations. The centreline turbulence intensity reaches a peak around $x/d = 8$ for the unexcited case. Under excitation, this peak increases and moves upstream to $x/d = 6$, as in the observations of Hussain & Thompson (1980), Hasan & Hussain (1980) and Favre-Marinet & Binder (1979).

The turbulence productions by the mean flow EI'_{Rs} and by the two coherent components $|A|^2 EI_{\mathrm{wt}}$ and $|B_1|^2 EI_{\mathrm{wt}}$ are shown in figure 17 for the same initial conditions as in figure 16. In the unforced case the figure shows that the turbulence production is mainly due to the mean flow. In the forced case the figure shows some turbulence production by the fundamental, and significant turbulence production by the subharmonic. The subharmonic streamwise lifespan is much larger than that of

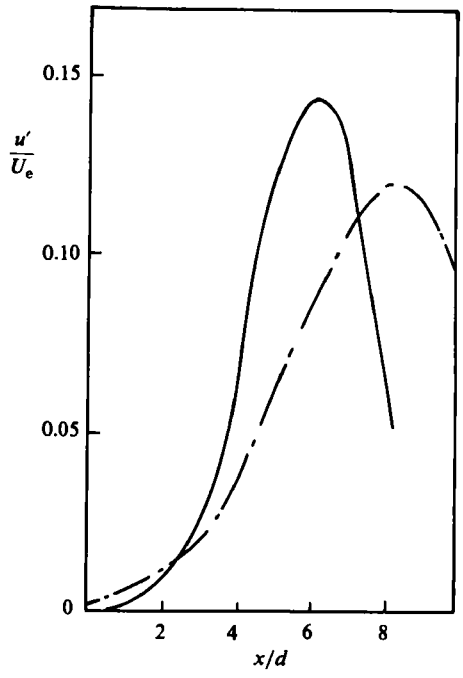

FIGURE 16. Random turbulence enhancement due to excitation at $St = 0.8$ and excitation level $\tilde{u}_f = 3\%\ U_e$: ——, excited; — — —, unexcited.

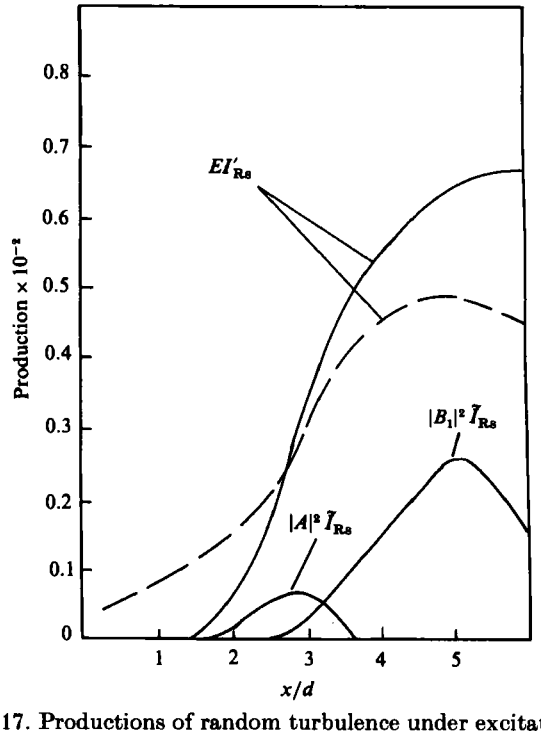

FIGURE 17. Productions of random turbulence under excitation at $St = 0.8$: excitation level $\tilde{u}_f = 3\%\ U_e$: ——, excited; – – – –, unexcited.

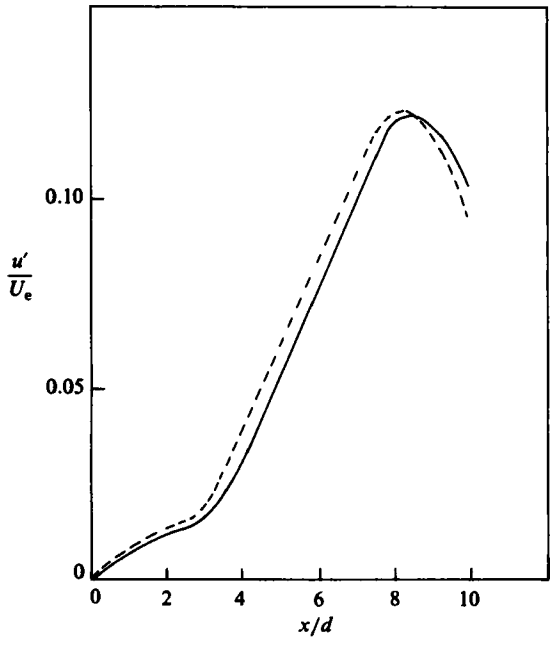

FIGURE 18. Random-turbulence suppression due to excitation at $St = 2.4$; excitation level 1% U_e: ——, excited; – – – –, unexcited.

the fundamental, and therefore it is more efficient in transferring energy to the random turbulence. As a result of excitation, the turbulence production by the mean flow EI'_{Rs} first decreases owing to the saturation of the meanflow by the fundamental component. But farther downstream the turbulence production by the mean flow in the excited case exceeds that of the unexcited case through increasing E, which results from the coherent-structure–random-turbulence interactions. Once the two coherent components have decayed, the turbulence production is governed by the mean flow alone, and the two governing mechanisms are EI'_{Rs} and the viscous dissipation $E^{\frac{3}{2}} I_\epsilon$.

Since pairing is viewed here as a consequence of the fundamental–subharmonic interaction, the role of pairing on the random turbulence enhancement can thus be divided into the following mechanisms: (i) through the fundamental, which absorbs energy from the mean flow as it grows, and subsequently pumps this energy as it decays to the random turbulence; (ii) the nonlinear growth of the fundamental results in amplification of the subharmonic, which in turn pumps significant energy from the mean flow to the random turbulence; (iii) as a result of these mechanisms, the turbulence intensity and hence its Reynolds stresses increase. This increases the direct production of turbulence by the mean flow. This mechanism is also suggested by Ho & Huang (1982), who speculated that the large strain rates resulting from the coalescence of the coherent structures are responsible for the generation of small-scale eddies. Browand & Weidman (1976) have also found that the pairing process was responsible for the production of Reynolds stresses.

7.2. *Turbulence suppression due to excitation*

At higher Strouhal numbers based on diameter several experimental observations have indicated that the turbulence can be suppressed. Vlasov & Ginevsky (1974) observed suppression of turbulence intensities in a circular jet under excitation at

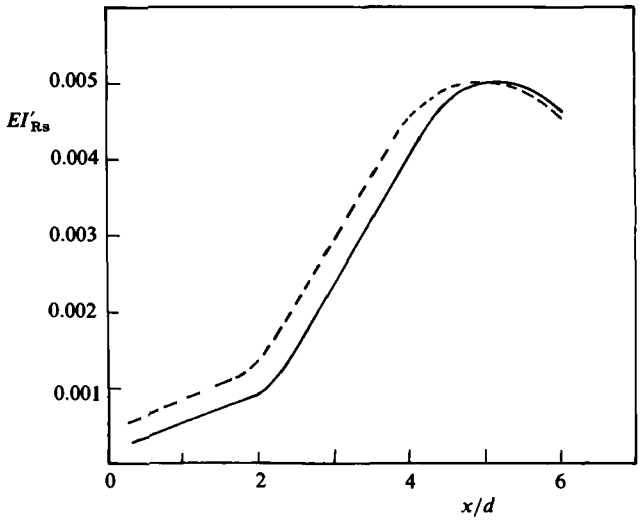

FIGURE 19. Productions of random turbulence due to excitation at $St = 2.4$; excitation level 1 % U_e. ——, excited; – – – –, unexcited.

$St = 2.75$ and that there is an optimum level of excitation for which the suppression is an optimum. Zaman & Hussain (1981) have also shown that suppression occurs for the St-range 1.2–2.4 and maximum suppression occurs when $St_\theta = 0.017$. In order to examine the mechanism of turbulence suppression in the present analysis, the random-turbulence axial velocity component along the jet centreline is shown in figure 18 for the unexcited case and for the case of excitation at $St = 2.4$. The initial conditions are $\theta_0 = 0.025d$, $u' = 0.3$ %, the subharmonic initial velocity level is 0.01 % U_e and the forcing level of $\tilde{u}_f$ is 3 % U_e. The figure shows some turbulence suppression, as in the observations of Vlasov & Ginevsky (1974), Petersen, Kaplan & Laufer (1974) and Zaman & Hussain (1981). However, the computed turbulence suppression is much less than the observed one. Figure 18 also shows that the location of the peak around $x/d \approx 8$ moves downstream as a result of suppression, which the observations of Zaman & Hussain (1981) have also indicated.

The turbulence productions by the mean flow and by the coherent components are shown in figure 19, for the same conditions as in figure 18. The figure shows that the dominant production term for both the excited and the unexcited cases is the mean-flow production, which is reduced as a result of excitation. The turbulence suppression can thus be explained as follows. The instability wave at a high Strouhal number has a much shorter streamwise lifespan as compared with the low-Strouhal-number instability waves. Therefore the former is much less efficient than the latter in pumping energy from the mean flow to the background turbulence. Excitation at high Strouhal numbers, e.g. $St \approx 2.4$, raises the level of the corresponding high-Strouhal number short instability wave and thus increases its energy drain from the mean flow. As in Ho & Huang's (1982) results, this excessive initial energy drain from the mean flow causes the momentum thickness to increase, and consequently the mean shear strain $\partial U/\partial r$ decreases. Therefore less mean-flow energy is available for the direct mean-flow production of the random turbulence. Thus, as a result of the loss of availability of mean-flow energy, the random turbulence is suppressed when the jet is excited at high Strouhal numbers.

8. Conclusions

The energy-integral technique was used to study the interactions between a fundamental instability component and its subharmonics in a turbulent round jet. Because of the assumed radial shapes and the finite number of wave components considered, the method is only approximate. Vortex pairing is viewed as the subharmonic's amplification resulting from its interaction with the fundamental. Excitation at low to moderate Strouhal numbers was found to result in amplifying the first subharmonic, which was found to be most pronounced if the excitation Strouhal number is in the range of 0.6–1.0. Excitation at higher Strouhal numbers was found to result in the amplification of several subharmonics.

The strength of the fundamental–subharmonic interactions, as measured by the subharmonic's amplification, was found to increase nonlinearly with increasing initial level of the forced fundamental. Beyond a certain level further increase in the initial level of the fundamental result in suppression of the amplification of the subharmonic and hence the vortex-pairing process. The fundamental's peak and the subharmonic's peak were found to move closer to the nozzle exit with increasing excitation Strouhal number. The location and the level of the fundamental's peak were found to be dependent on the uncontrolled initial level of the subharmonic and on its initial phase difference with respect to the fundamental. This can explain the observed irregularity or jitter in pairing.

A study of the energy exchanges between the different flow components along the jet indicated that the importance of each of the mechanisms governing the growth and decay of coherent components under excitation depends on the Strouhal number and on the streamwise location. At moderate Strouhal numbers the fundamental's production by the mean flow is the dominant mechanism close to the nozzle exit. The fundamental subsequently decays through three equally significant mechanisms: turbulence damping, generation of its first subharmonic, and negative production in which energy is transferred from the coherent component to the mean flow. The fundamental amplifies the subharmonic through two mechanisms. First, it pumps energy from the mean flow to the subharmonic. Secondly, the enhanced level of the subharmonic acts as a catalyst that increases the direct mean-flow production of the subharmonic. The first subharmonic subsequently decays mainly through turbulence damping. At high Strouhal numbers the fundamental grows by absorbing energy from the mean flow and decays through negative production and through generating its first subharmonic. The first subharmonic grows as a result of its production by both the mean flow and by the fundamental, and decays as a result of its negative production and as a result of generating the second subharmonic. The subsequent subharmonics behave similarly, but the significance of the negative-production decay mechanism diminishes as the Strouhal number of the subharmonic decreases. The low-Strouhal-number subharmonics decay basically through turbulence damping.

As a result of the energy transfer from the coherent components to the random turbulence, the turbulence intensity is enhanced when the jet is excited at moderate Strouhal numbers. If the excitation Strouhal number is high, the streamwise lifespans of the coherent components are short, and therefore they pump negligible energy to the random turbulence. Thus, as a result of initial mean-flow energy drain for the growth of the coherent components, less mean-flow energy is available for the production of turbulence. Consequently the turbulence is suppressed when the jet is excited at high Strouhal numbers. The close agreement between theory and observations suggests that a nonlinear fundamental–subharmonic interaction mechanism can explain the observed vortex-pairing phenomena.

The author wishes to express his gratitude to Professor J. T. C. Liu of Brown University for his enlightening discussions. The author is also indebted to Professors D. G. Crighton, A. K. M. F. Hussain, C. M. Ho, A. Michalke, P. A. Monkewitz, and to Drs V. Kibens, G. L. Morrison and K. B. M. Q. Zaman for supplying experimental data for comparisons.

This work is partly supported by the office of Naval Research through grant SIT-4-25464 and the University's Research Council Fund of Rutgers University through grant URF-G-84-650-NB-14.

REFERENCES

ACTON, E. 1976 *J. Fluid Mech.* **76**, 561.

ACTON, E. 1980 *J. Fluid Mech.* **98**, 1.

AHUJA, K. K., LEPICOVSKY, J. & BURRIN, R. H. 1982 *AIAA J.* **20**, 1700.

ARBEY, H. & FFOWCS-WILLIAMS, J. E. 1984 *AIAA Paper* 84-2338.

BALTAS, C. & MORRIS, P. J. 1984 *AIAA Paper* 84-2342.

BRADSHAW, P., FERRIS, D. H. & JOHNSON, R. F. 1964 *J. Fluid Mech.* **19**, 591.

BROWAND, F. K. & HO, C.-M. 1983 In *Two-Dimensional Turbulence* (*J. Méc. Numéro Spécial*), p. 99.

BROWAND, F. K. & LATIGO, B. O. 1979 *Phys. Fluids* **22**, 1011.

BROWAND, F. K. 1980 In *Proc. 33rd Ann. Meeting Div. Fluid Dyn., APS.*

BROWAND, F. K. & WEIDMAN, P. D. 1976 *J. Fluid Mech.* **76**, 127.

BROWN, G. L. & ROSHKO, A. 1974 *J. Fluid Mech.* **64**, 775.

CORCOS, G. M. & LIN, S. J. 1984 *J. Fluid Mech.* **139**, 29.

CORCOS, G. M. & SHERMAN, F. S. 1976 *J. Fluid Mech.* **73**, 241.

CRIGHTON, D. G. & GASTER, M. 1976 *J. Fluid Mech.* **77**, 397.

CROW, S. C. & CHAMPAGNE, F. H. 1971 *J. Fluid Mech.* **48**, 547.

DAVIES, P. O. A. L., FISHER, M. J. & BARRATT, J. J. 1963 *J. Fluid Mech.* **15**, 337.

DRUBKA, R. G. 1981 Ph.D. thesis, Illinois Institute of Technology, Chicago.

FAVRE-MARINET, M. & BINDER, G. 1979 *J. Méc.* **18**, 356.

FREYMUTH, P. 1966 *J. Fluid Mech.* **25**, 603.

GUTMARK, E. & HO, C. M. 1983 *Phys. Fluids* **26**, 2932.

HASAN, M. A. Z. & HUSSAIN, A. K. M. F. 1980 *Internal Rep., Univ. Houston.*

HINZE, J. O. 1975 *Turbulence*, pp. 489–495. McGraw-Hill.

HO, C. M. & HUANG, L. S. 1982 *J. Fluid Mech.* **119**, 443.

HO, C. M. & HUERRE, P. 1984 *Ann. Rev. Fluid Mech.* **16**, 365.

HUERRE, P. 1980 *Phil. Trans. R. Soc. Lond.* A **293**, 643.

HUSAIN, Z. D. & HUSSAIN, A. K. M. F. 1983 *AIAA J.* **21**, 1512.

HUSSAIN, A. K. M. F. & REYNOLDS, W. C. 1970 *J. Fluid Mech.* **41**, 241.

HUSSAIN, A. K. M. F. & THOMPSON, C. A. 1980 *J. Fluid Mech.* **100**, 397.

KELLY, R. E. 1967 *J. Fluid Mech.* **27**, 657.

KENDALL, J. M. 1970 *J. Fluid Mech.* **41**, 259.

KIBENS, V. 1980 *AIAA J.* **18**, 434.

KIBENS, V. 1981 *AIAA Paper* 81-1960.

KNIGHT, D. C. 1979 In *Proc. 6th Symp. on Turbulence in Liquids, Univ. Missouri, Rolla*, p. 167.

KO, D. R. S., KUBOTA, T. & LEES, L. 1970 *J. Fluid Mech.* **40**, 315.

KO, N. W. M. & DAVIES, P. O. A. L. 1971 *J. Fluid Mech.* **50**, 40.

LAUFER, J. & YEN, T.-C. 1983 *J. Fluid Mech.* **134**, 1.

LAUFER, J. & ZHANG, J. X. 1983 *Phys. Fluids* **26**, 1740.

LIU, J. T. C. 1971 *Phys. Fluids* **14**, 2251.

LIU, J. T. C. 1974 *J. Fluid Mech.* **62**, 437.

MANKBADI, R. & LIU, J. T. C. 1981 *Phil. Trans. R. Soc. Lond.* A **298**, 541.

MANKBADI, R. & LIU, J. T. C. 1984 *Phil. Trans. R. Soc. Lond.* A **311**, 183.

MICHALKE, A. 1965 *J. Fluid Mech.* **23**, 521.

MICHALKE, A. 1971 *Z. Flugwiss.* **19**, 319.

MONKEWITZ, P. A. 1982 *Internal Rep., Univ. California Los Angeles.*

MOORE, C. J. 1977 *J. Fluid Mech.* **80**, 321.

MORRIS, P. J. 1976 *J. Fluid Mech.* **77**, 511.

OSTER, D. & WYGNANSKI, I. 1982 *J. Fluid Mech.* **123**, 91.

PATNAIK, P. A., SHERMAN, F. S. & CORCOS, G. M. 1976 *J. Fluid Mech.* **73**, 215.

PETERSEN, R. A., KAPLAN, R. G. & LAUFER, J. 1974 *NASA Contractors Rep.* 134733.

PLASCHKO, P. 1979 *J. Fluid Mech.* **92**, 209.

REYNOLDS, W. C. & BOUCHARD, E. E. 1981 In *Unsteady Turbulent Shear Flows* (ed. R. Michel, J. Cousteix & R. Houdeville), p. 402. Springer.

REYNOLDS, W. C. & HUSSAIN, A. K. M. F. 1972 *J. Fluid Mech.* **24**, 263.

RILEY, J. J. & METCALFE, R. W. 1980 *AIAA Paper* 80-0274.

STUART, J. T. 1958 *J. Fluid Mech.* **4**, 1.

STUART, J. T. 1960 *J. Fluid Mech.* **9**, 353.

STUART, J. T. 1965 *Appl. Mech. Rev.* **18**, 523.

STRANGE, P. J. R. & CRIGHTON, D. G. 1983 *J. Fluid Mech.* **134**, 231.

VLASOV, Y. V. & GINEVSKY, A. S. 1974 *NASA* TTF-15,721.

WINANT, C. D. & BROWAND, F. K. 1974 *J. Fluid Mech.* **63**, 237.

WLEZIEN, R. W. & KIBENS, V. 1984 *AIAA paper presented at the Aerosp. Sci. Meeting, Reno, NV.*

ZAMAN, K. B. M. Q. & HUSSAIN, A. K. M. F. 1980 *J. Fluid Mech.* **101**, 449.

ZAMAN, K. B. M. Q. & HUSSAIN, A. K. M. F. 1981 *J. Fluid Mech.* **103**, 133.

ZHANG, Y.-Q., HO, C.-M. & MONKEWITZ, P. A. 1984 In *Proc. IUTAM Symp. on Laminar–Turbulent Transition, Novosibirsk.*